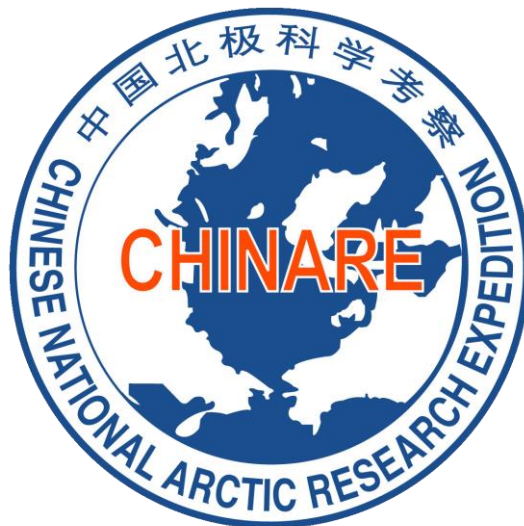


**Scientific Report of
the 10th Chinese Arctic Research Expedition (2019)
in the U.S. EEZ**



The 10th Chinese Arctic Research Expedition

30 April, 2022

Content

1.	Dominating figures	1
2.	Primary mission	2
3.	Investigation items	2
4.	Daily reports	3
5.	Primary results of data/sampling analysis	8
5.1	Meteorology and Physical Oceanography	8
5.2	Marine Chemistry	16
5.3	Marine Biology	22
5.4	Marine Geology	34
6.	Data submission	40
7.	Highlights of research results	42
7.1	Vertical distribution of nutrient tracers in the western Arctic.....	42
7.2	Neritic tintinnid community structure and vertical mixing	45
7.3	Planktonic ciliate community differences in 2016 and 2019	48
7.4	Meridional Variation of picophytoplankton.....	51
7.5	Grain size implications for sediment source and sink	53

1. Dominating figures

Chief Scientist:

Zexun Wei

No. 6 Xianxialing Road, Qingdao, Shandong, 266061

The First Institute of Oceanography,

Ministry of Natural Resources

Email: weizx@fio.org.cn

Associate Chief Scientist:

Hongxia Chen

No. 6 Xianxialing Road, Qingdao, Shandong, 266061

The First Institute of Oceanography,

Ministry of Natural Resources

Email: chenhx@fio.org.cn

2. Primary mission

Founded by the Chinese Polar Environment Comprehensive Investigation & Assessment Programme (2016-2020), Chinese Arctic and Antarctic Administration, the 10th Chinese National Arctic Research Expedition focuses on the change in Arctic sea ice and its influence on the environment and the ecosystem, the main characters of multi-scale ocean-ice-atmosphere interactions and climate changes. The cruise was carried out during 10 August to 26 September, 2019. The field work in the U.S. EEZ was a part of this cruise.

3. Investigation items

During this expedition, field works of physical oceanography, meteorology, marine chemistry, marine biology and marine geology are occupied in the Bering Sea and the Chukchi Sea.

Ship-based measurements of Station such CTD/LADCP/SVP profiling and Rosset water sampling, sediments sampling, phytoplankton net, and zooplankton net sampling, and underway observation and sampling of meteorological parameters and surface T/S were carried out.

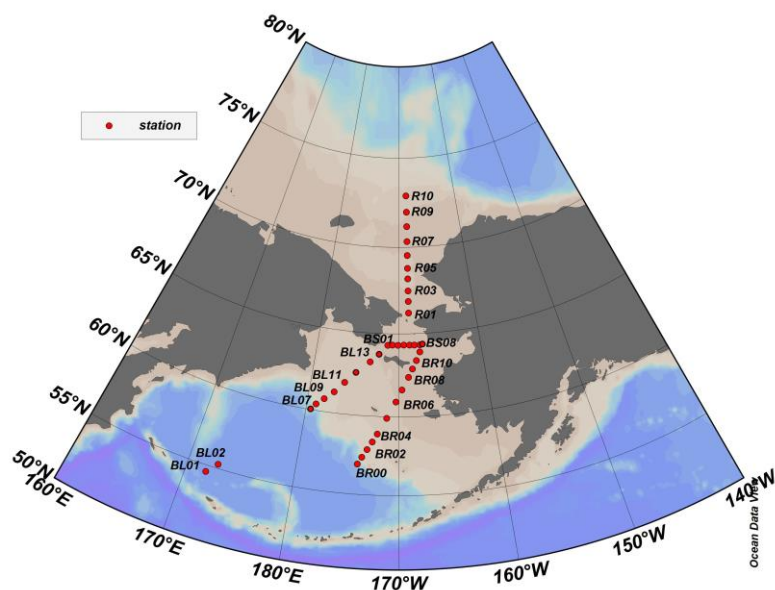


Fig. 3-1 Marine stations in the U.S. EEZ during the 10th CHINARE

4. Daily reports

The field works of CHINARE-2019 in the U.S. EEZ lasted from 24 August to 10 September. According to the Letter of Acknowledgement (LOA 2019-11) issued by the United States Department of Commerce-National Oceanic and Atmospheric Administration, we made a daily report for the operations of our Marine Scientific Research (MSR) in the U.S. EEZ to the Arctic Waterways Safety Committee, the Alaska Eskimo Whaling Commission, Kawerak Inc. to ensure no conflicts with subsistence harvesting.

The daily cruise log can be referred to Table 4-1 to Table 4-9. The *R/V Xiangyanghong 01* navigated from 54.59°N, 171.9°W at 24 August to start the field work in the U.S. EEZ. We finished all the MSR stations in the U.S. EEZ by 9 September 2019. In total, 40 MSR stations have been conducted in the U.S. EEZ.

Due to a sudden emergency, bad weather and time limitation etc., the sections in U.S. EEZ except the R section in the Arctic Ocean was

cancelled and we left the Bering Sea ahead of schedule.

Table 4-1. Cruise log on 24 August, 2019

No.	Station	Longitude (°E)	Latitude (°N)	Water depth (m)	Observation or investigation
1	BL01	171.9	54.59	3867	CTD+LADCP+SVP+Rosette Sampler, Phytoplankton net, Zooplankton net, Micro-plastics Trawl

Table 4-2. Cruise log on 25 August, 2019

No.	Station	Longitude (°E)	Latitude (°N)	Water depth (m)	Observation or investigation
1	BL02	172.78	55.27	3866	CTD+LADCP+SVP+ Rosette Sampler

Table 4-3. Cruise log on 28 August, 2019

No.	Station	Longitude (°E)	Latitude (°N)	Water depth (m)	Observation or investigation
1	BL07	-179.5	60.04	2293	CTD+LADCP+SVP+ Rosette Sampler, planktonic sampling (Vertical trawling)
2	BL08	-179	60.4	1435	CTD+LADCP+SVP+ Rosette Sampler, Sediment sampling, Micro-plastics Trawl
3	BL09	-178.2	60.8	273	CTD+LADCP+SVP+ Rosette Sampler, Sediment sampling, planktonic sampling (Horizontal trawling +Vertical trawling)
4	BL10	-177.23	61.29	129	CTD+LADCP+SVP+ Rosette Sampler, Sediment sampling, Micro-plastics Trawl
5	BL11	-176.17	61.93	113	CTD+LADCP+SVP+ Rosette Sampler, Sediment sampling

Table 4-4. Cruise log on 29 August, 2019

No.	Station	Longitude (°E)	Latitude (°N)	Water depth (m)	Observation or investigation
1	BL12	-175	62.6	80	CTD+LADCP+SVP+ Rosette Sampler, Sediment sampling, Planktonic sampling (Horizontal trawling +Vertical trawling)

No.	Station	Longitude (°E)	Latitude (°N)	Water depth (m)	Observation or investigation
2	BL13	-173.43	63.29	65	CTD+LADCP+SVP+ Rosette Sampler, Sediment sampling
3	BL14	-172.4	63.77	55	CTD+LADCP+SVP+ Rosette Sampler, Sediment sampling, Planktonic sampling (Horizontal trawling +Vertical trawling)
4	BS01	-171.39	64.33	39	CTD+LADCP+SVP+ Rosette Sampler, Micro-plastics Trawl
5	BS02	-170.81	64.33	45	CTD+LADCP+SVP+ Rosette Sampler, planktonic sampling (Vertical trawling)
6	BS03	-170.12	64.33	43	CTD+LADCP+SVP+ Rosette Sampler

Table 4-5. Cruise log on 30 August, 2019

No.	Station	Longitude (°E)	Latitude (°N)	Water depth (m)	Observation or investigation
1	BS04	-169.4	64.33	38	CTD+LADCP+SVP+ Rosette Sampler
2	BS05	-168.7	64.33	40	CTD+LADCP+SVP+ Rosette Sampler, Phytoplankton net, Zooplankton net, Benthic Trawl
3	BS06	-168.09	64.33	35	CTD+LADCP+SVP+ Rosette Sampler
4	BS07	-167.46	64.33	30	CTD+LADCP+SVP+ Rosette Sampler, Micro-plastics Trawl
5	BS08	-166.96	64.33	29	CTD+LADCP+SVP+ Rosette Sampler, Phytoplankton net, Zooplankton net, Benthic Trawl
6	R01	-168.75	66.2	52	CTD+LADCP+SVP+ Rosette Sampler, Surface sediments (box core), Micro-plastics Trawl
7	R02	-168.75	66.9	46	CTD+LADCP+SVP+ Rosette Sampler, sediments sampling, Phytoplankton net, Zooplankton net, Benthic Trawl

Table 4-6. Cruise log on 31 August, 2019

No.	Station	Longitude (°E)	Latitude (°N)	Water depth (m)	Observation or investigation
1	R03	-168.75	67.5	51	CTD+LADCP+SVP+Rosette Sampler, Surface sediments (box core)

2	R04	-168.75	68.2	62	CTD+LADCP+SVP+Rosette Sampler, Surface sediments (box core), Benthic Trawls
3	R05	-168.75	68.8	53	CTD+LADCP+SVP+Rosette Sampler, Surface sediments (box core), Micro-plastics Trawl
4	R06	-168.75	69.54	52	CTD+LADCP+SVP+Rosette Sampler, Surface sediments (box core), Phytoplankton net, Zooplankton net, Benthic Trawl
5	R07	-168.75	70.34	38	CTD+LADCP+SVP+Rosette Sampler, Surface sediments (box core), Phytoplankton net, Zooplankton net, Benthic Trawl

Table 4-7. Cruise log on 1 September, 2019

No.	Station	Longitude (°E)	Latitude (°N)	Water depth (m)	Observation or investigation
1	R08	-168.75	71.18	48	CTD+LADCP+SVP+Rosette Sampler, Surface sediments (box core),
2	R09	-168.75	71.99	50	CTD+LADCP+SVP+Rosette Sampler, Surface sediments (box core), Micro-plastics Trawl
3	R10	-168.75	72.9	84	CTD+LADCP+SVP+Rosette Sampler, Surface sediments (box core), Phytoplankton net, Zooplankton net, Benthic Trawl

Table 4-8. Cruise log on 7 September 2019

No.	Station	Longitude (°E)	Latitude (°N)	Water depth (m)	Observation or investigation
1	BR06	-170.35	60.9	40	CTD+LADCP+SVP+Rosette Sampler, Surface sediments (box core)
2	BR07	-169.69	61.66	36	CTD+LADCP+SVP+Rosette Sampler, Surface sediments (box core), Micro-plastics Trawl
3	BR08	-168.91	62.4	37	CTD+LADCP+SVP+Rosette Sampler, Surface sediments (box core)
4	BR09	-168.44	62.9	42	CTD+LADCP+SVP+Rosette Sampler, Surface sediments (box core), Phytoplankton net, Zooplankton net, Benthic Trawl
5	BR10	-167.96	63.4	25	CTD+LADCP+SVP+Rosette Sampler, Surface sediments (box core)
6	BR11	-167.48	63.9	34	CTD+LADCP+SVP+Rosette Sampler, Surface sediments (box core), Phytoplankton net, Zooplankton net, Benthic Trawl

Table 4-9. Cruise log on 8 September 2019

No.	Station	Longitude (°E)	Latitude (°N)	Water depth (m)	Observation or investigation
1	BR00	-174.09	56.95	145	CTD+LADCP+SVP+Rosette Sampler, Surface sediments (box core)
2	BR01	-173.7	57.4	124	CTD+LADCP+SVP+Rosette Sampler, Surface sediments (box core)
3	BR02	-173.22	57.9	93	CTD+LADCP+SVP+Rosette Sampler, Surface sediments (box core), Phytoplankton net, Zooplankton net, Benthic Trawl
4	BR03	-172.74	58.4	115	CTD+LADCP+SVP+Rosette Sampler, Surface sediments (box core), Micro-plastics Trawl
5	BR04	-172.26	58.9	59	CTD+LADCP+SVP+Rosette Sampler, Surface sediments (box core)
6	BR05	-171.31	59.9	62	CTD+LADCP+SVP+Rosette Sampler, Surface sediments (box core), Phytoplankton net, Zooplankton net, Benthic Trawl

5. Primary results of data/sampling analysis

5.1 Meteorology and Physical Oceanography

Coordinators:

Yan He (Physical oceanography)

No. 6 Xianxialing Road, Qingdao, Shandong, 266061

The First Institute of Oceanography,

Ministry of Natural Resources

Email: heyan@fio.org.cn

Xiaoping Mai (Meteorology)

No. 8 Dahuisi Road, Beijing, 100083

National Marine Environmental Forecasting Center,

Ministry of Natural Resources

Email: maixp18@nmefc.cn

5.1.1 Meteorology

The ship-based meteorological observations on the cruise in the U.S.EEZ lasted from 24 August to 9 September, and the cloud, visibility, wind speed and direction, sea surface temperature and humidity, sea level pressure, wave and swell heights were recorded on the 00UTC, 06UTC and 12UTC each day.

There were three cyclone events occurring during the field works on 2 to 4, 5 to 6, and 7 to 8 September, respectively. The sea level pressure ranged from 994 to 1024 hPa (Fig. 5-1). The near surface air temperature ranged from 1.1° to 15.8°C (Fig. 5-2). The wind speed ranged from 1.0 to 13.8 m/s, with the dominant direction from the east or southeast and the Beaufort wind scale 5 dominating (Fig. 5-3 and Fig. 5-4). Moreover, we

suffered two dense fog events.

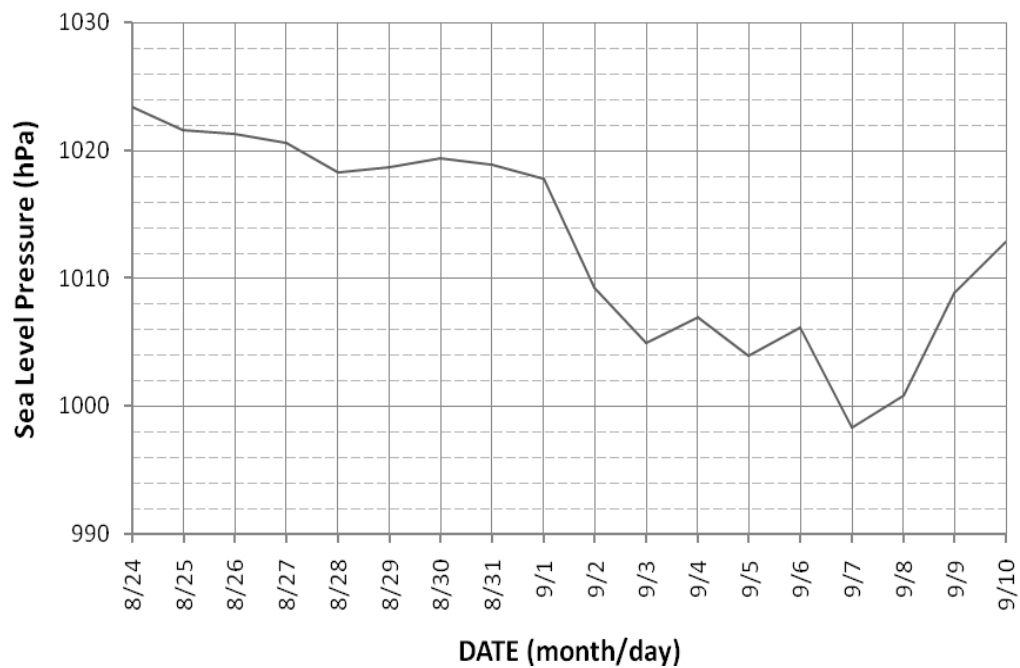


Fig. 5-1 Time series of daily mean sea level pressure in the U.S. EEZ

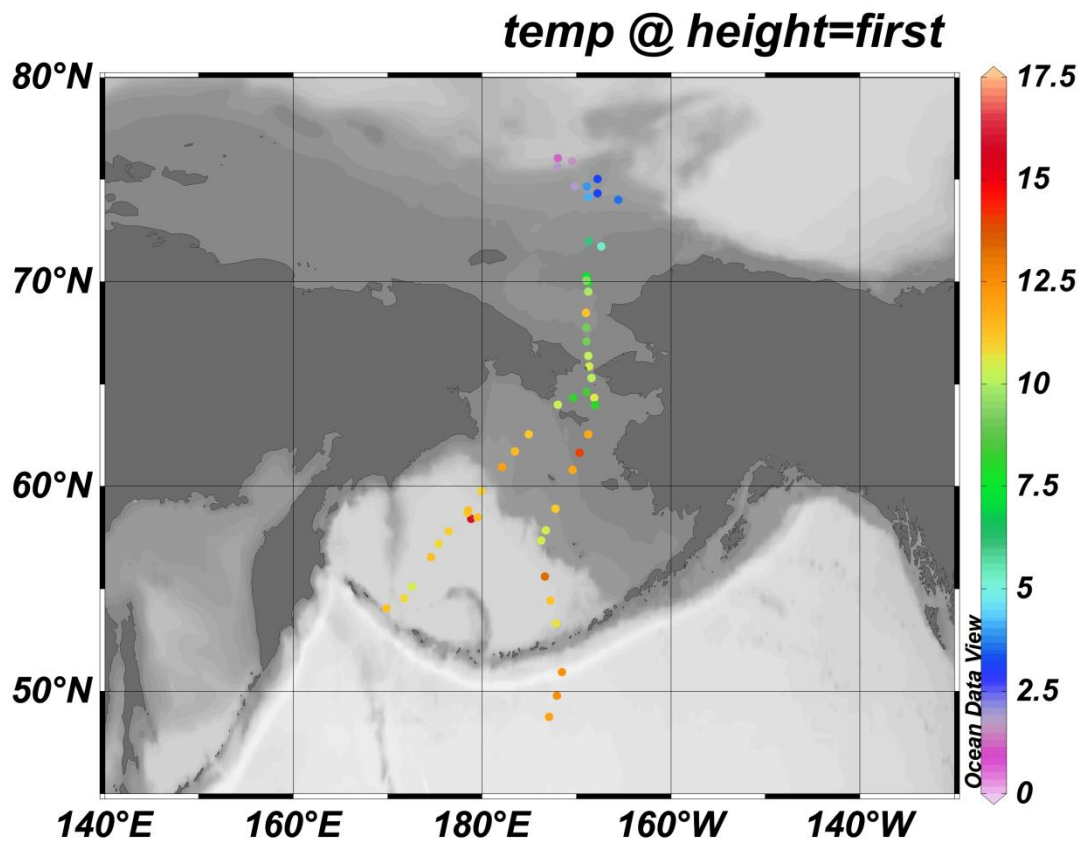


Fig. 5-2 Tracks of air temperature (°C) in the U.S. EEZ

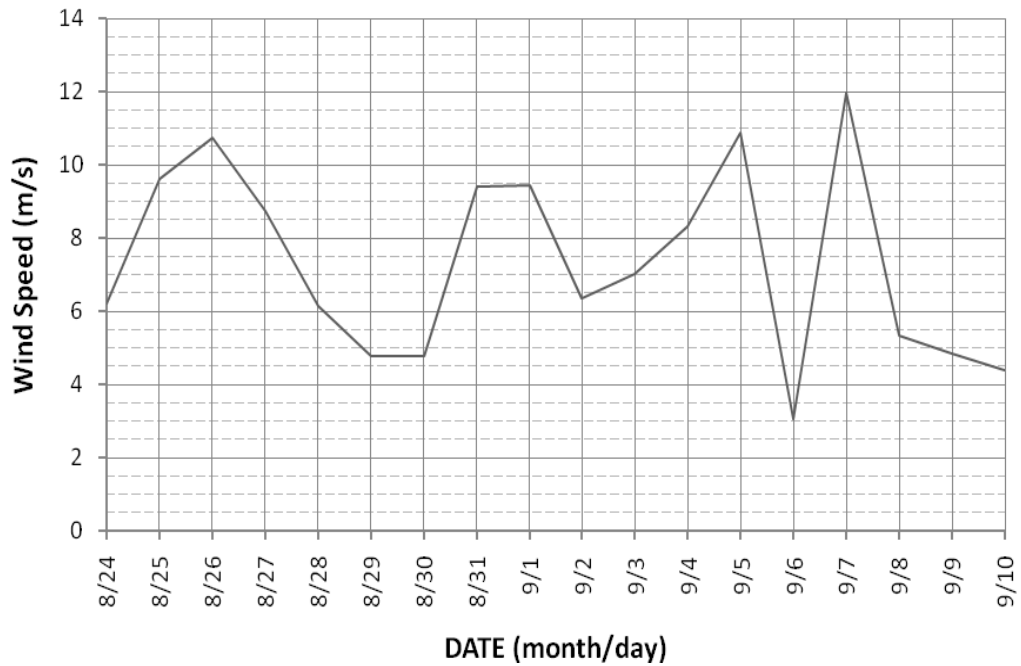


Fig. 5-3 Time series of daily mean wind speed in the U.S. EEZ

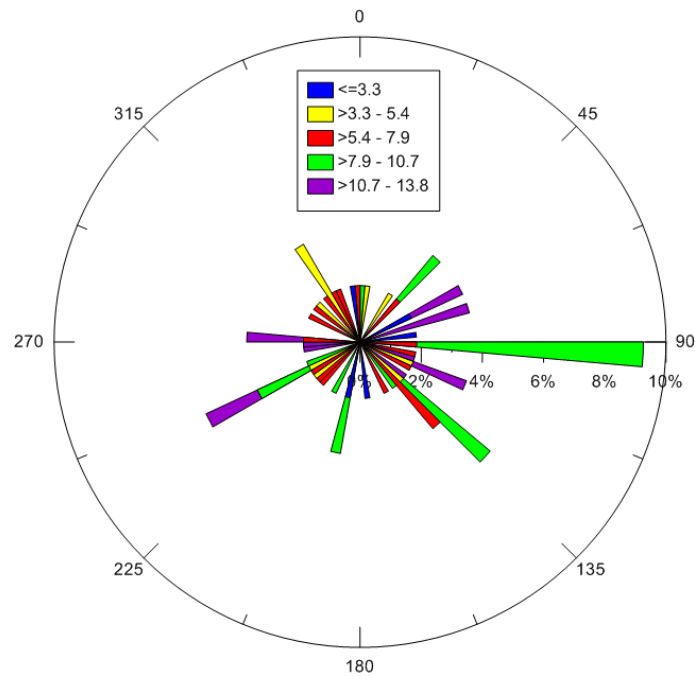


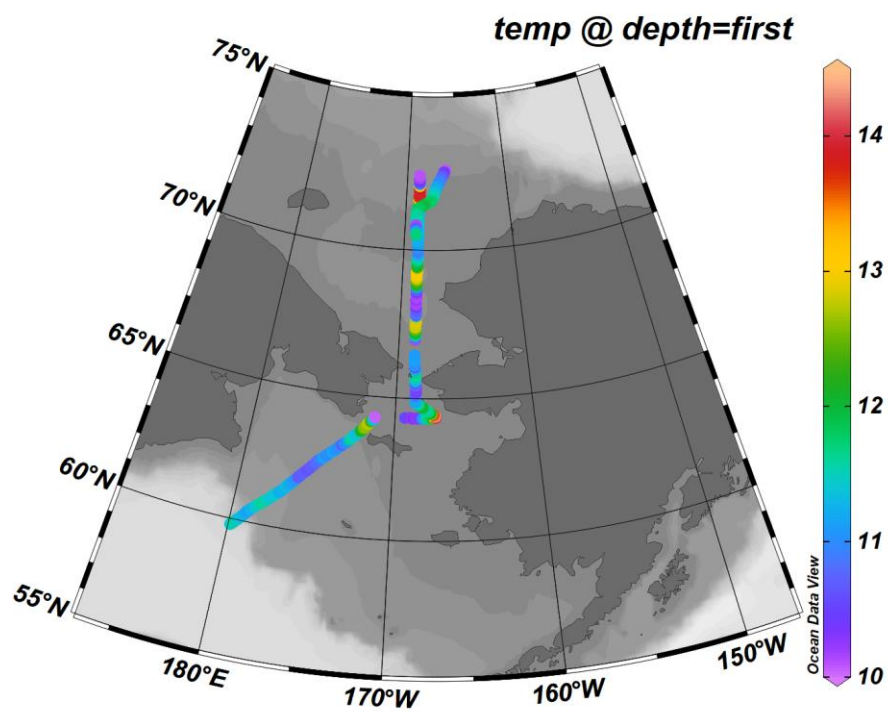
Fig. 5-4 Wind speed (m/s) and direction distribution in the U.S. EEZ

5.1.2 Physical oceanography

Ocean surface is the interface to exchange material and energy between the atmosphere and ocean. The temperature and salinity are the two key factors for the changes in the atmosphere-ocean system. So, the observations of the surface temperature and salinity during the cruise will

be beneficial not only to the enriching of the observation data, but also to the understanding of the atmosphere-ocean interaction processes.

The trajectories colored by surface temperature and salinity in the Bering Sea and Chukchi Sea are shown in Fig. 5-5. The sea surface salinities were relatively high in the Bering Sea and Bering Strait, in which the salinities were above 31. The salinities decreased across the Bering Strait, though there were some areas where salinities were relatively high. Compared to salinities, the temperature difference between the Bering Sea and Chukchi Sea was small.



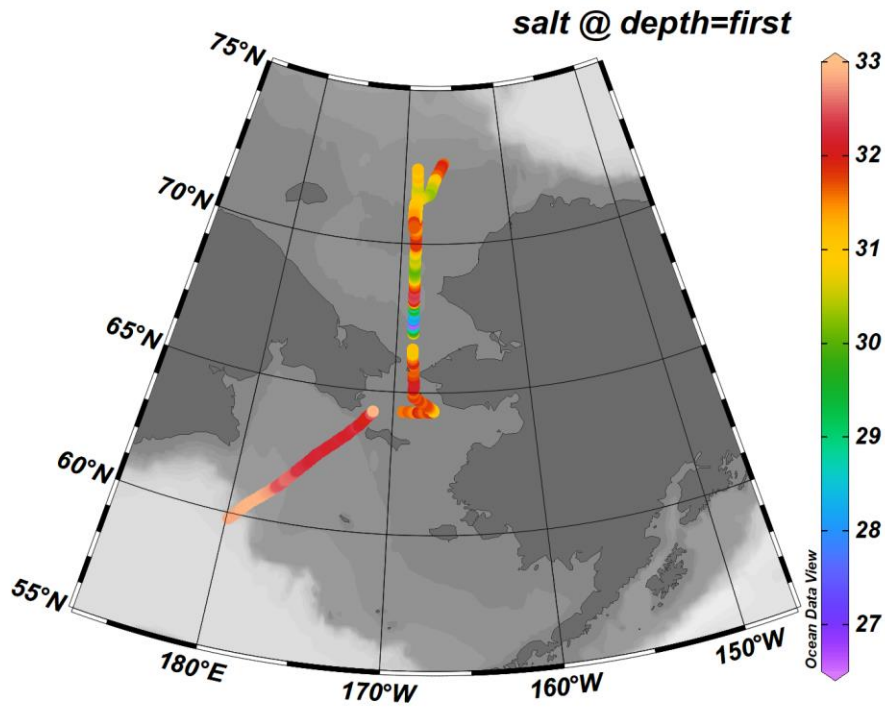


Fig. 5-5 Trajectory colored by sea surface temperature (upper panel, °C) and salinity (lower panel, PSU)

One of the main instruments for the oceanographic survey is the SBE 911plus CTD, which is a high-precision temperature-salinity-depth measurement system produced by American Sea-Bird Electronics, Inc. The system is equipped with sensors of double temperature, double conductivity, dissolved oxygen, pressure, chlorophyll and altimeter. The current was measured by the Acoustic Doppler Current Profiler, which was produced by American RDI Company. During the expedition, the ADCP was bundled with SBE 911Plus CTD system for the observation. During this expedition, 40 observation stations for ocean temperature, salinity and depth (CTD) profiling and current velocity profiling (Lowed-ADCP) were carried out.

During August 30-31, our research R/V Xiangyanghong 01 sailed across the Bering Strait and into the Arctic Ocean. We conducted a south-north CTD section, sailing from the Bering Strait to the northern

Chukchi Sea which we named as the “R section”. Fig. 5-6 shows a strong halocline at the depth of 20 m with warm/fresh water above and cold/saline water below. The warm and fresh water above could be the mixture of sea ice melt water and river runoff. The sunlight provides the heat energy to warm it up. There is a clear temperature boundary at 69.5°N below the depth of 20 m with warmer water in the south and colder water in the north. The relatively warm Pacific Water in the southern section represents the newly Pacific Summer Water, while the cold water (temperature approaches the freezing point) in the north has the properties of Pacific Winter Water. There show distinct warm and relatively fresh water properties for stations R05 and R06. This anomalous warm water extends from the surface down to the ocean bottom. This calls for further investigation. It could be an eddy or just because the R section went across different Pacific Water branches. This anomalous water could be the core of one branch. During September 6-8, our research vessel conducted a CTD section from the northern Bering Sea to the south (Fig. 5-7).

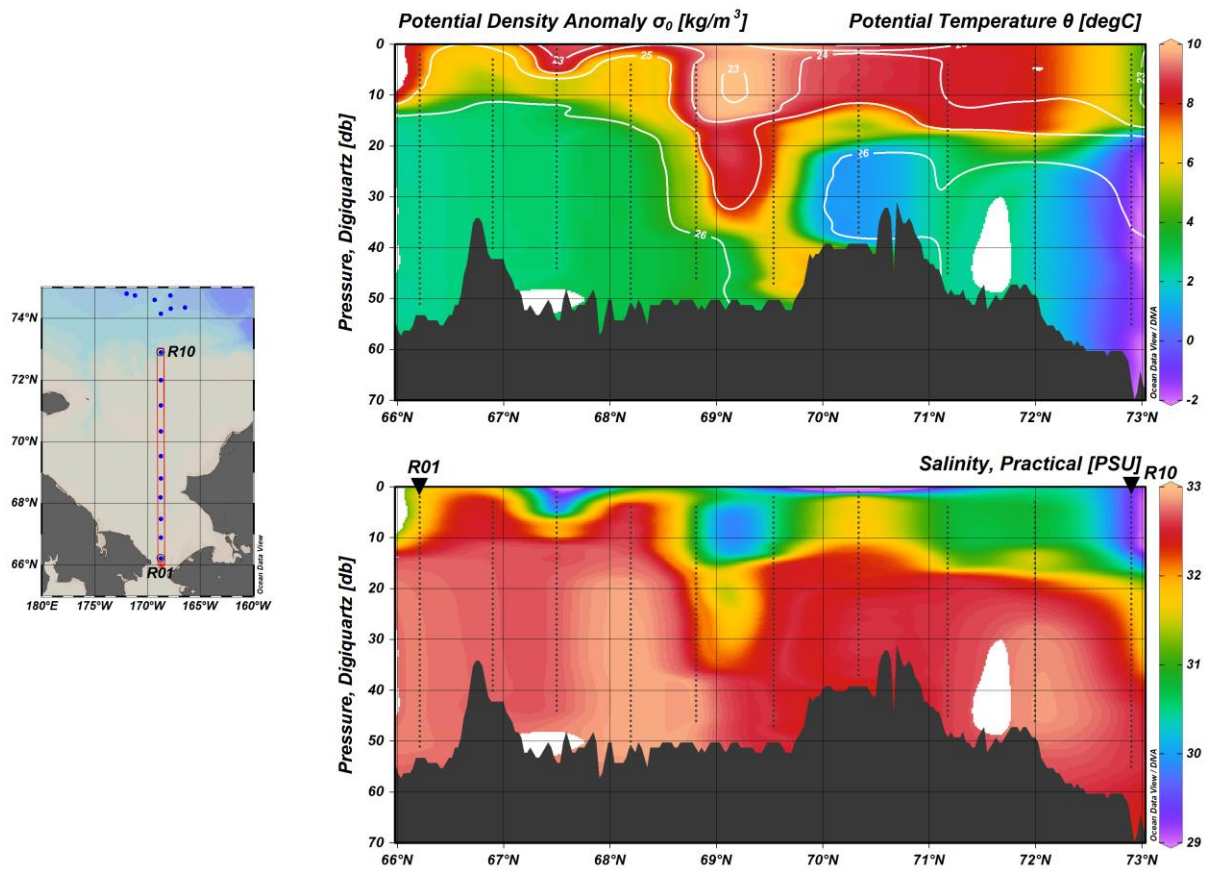


Fig. 5-6 The potential temperature, salinity and potential density for the R section across the Chukchi Sea.

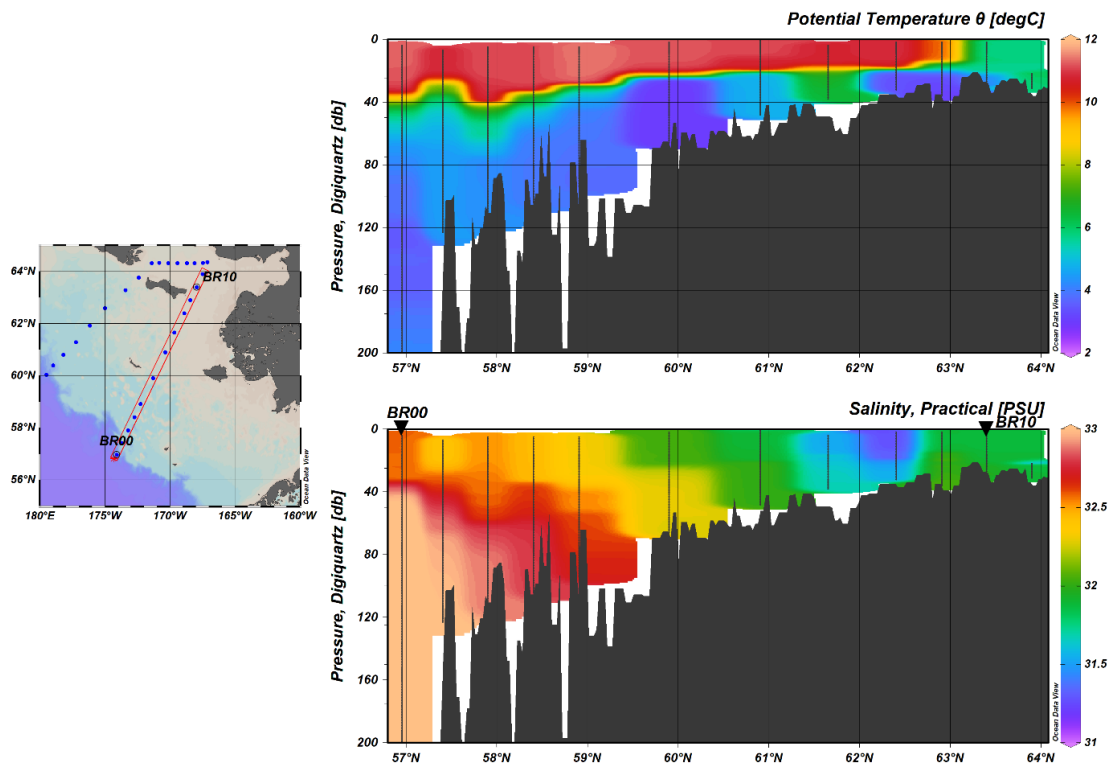


Fig. 5-7 The potential temperature, salinity and potential density for the BR section that across the Bering Sea.

The current observation is mainly conducted using a 300k Hz lowered ADCP, which is a high-precision ocean current measurement system. As it can be seen from the Fig. 5-8, the current velocity at the bottom of station R10 is relatively high, and the direction of upper and lower laminar flow is opposite, with a strong shear.

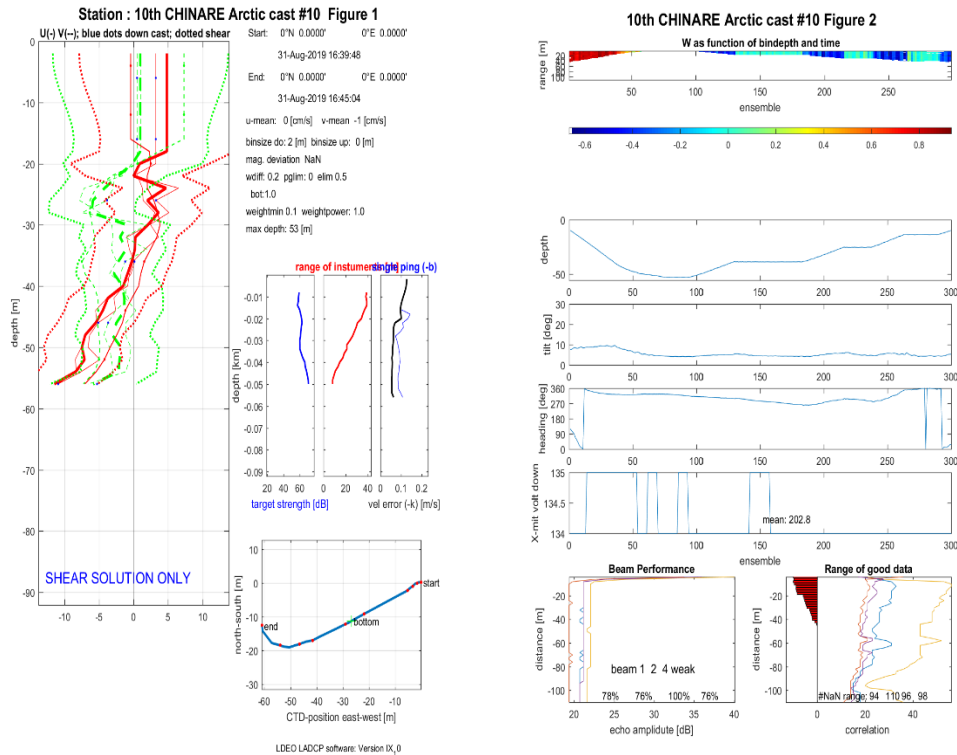


Fig. 5-8 The speed of the current of the section R10

Sound speed in water was directly measured by a Sound Velocity Profiler (SVP), which was bundled with SBE 911Plus CTD system for observation. During this cruise, 40 stations for sound speed profiling were carried out. Fig. 5-9 show variations in the sound speed for different depths at some stations. In the Bering Sea, the sound speed in the upper mixed layer was around 1490 m/s, and the minimum sound speed (lower than 1460 m/s) occurred at the depth of 40-60 m. The sound speed in surface water was around 1440m/s in the Arctic Ocean, and it reached

minimum at about 40 m depth.

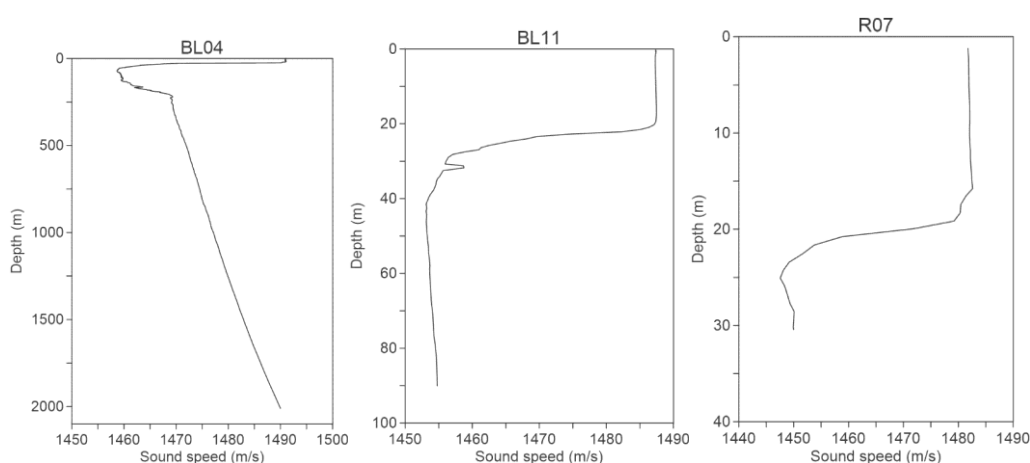


Fig. 5-9 Sound speed profiling at some stations

5.2 Marine Chemistry

Coordinator:

Yanpei Zhuang

No. 36 Baochubei Road, Hangzhou, Zhejiang, 310012

The Second Institute of Oceanography,

Ministry of Natural Resources

Email: Zhuangyp@sio.org.cn

Marine chemistry investigations were conducted at 40 sampling stations during the field work in the U.S. EEZ. Nitrate, soluble reactive phosphate, silicate, nitrite, and ammonia were collected and measured at 40 sampling stations. Dissolved oxygen were collected and measured at 35 sampling stations.

The BS transect can be considered as the most important section, because it had been observed during each CHINARE cruise. As showed in Fig. 5-10, the horizontal distribution of nitrite along the BS transect had no obvious difference, however, all the stations showed the similar vertical distribution, with the nitrite in the water column increased

obviously through the depth. The maximum of 0.20 $\mu\text{mol/L}$ was found in the ground water of BS02. The BS transect was located at the Bering Sea Shelf area, with Anadyr Current, Bering Shelf Current and Alaska Coastal Current distributed from west to the east. Therefore, the distribution of the nutrients at this area was influenced not only by the regeneration of the nutrients in the surface sediment, but also by those three currents and the river input, which appeared to be very complicated.

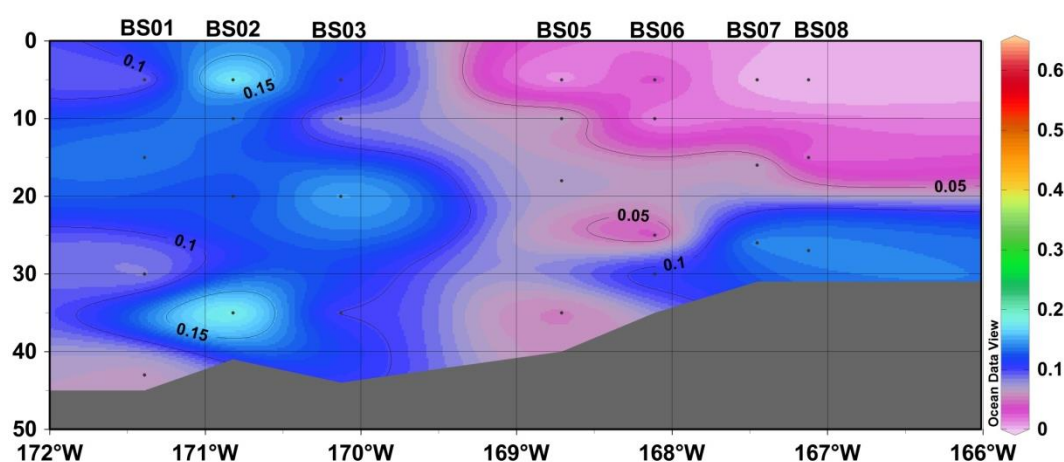


Fig. 5-10 Distribution of nitrite ($\mu\text{mol/L}$) along the BS transect in the Bering Sea

The maximum of 3.14 $\mu\text{mol/L}$ in the BS transect was found in the bottom water of BS03 station, which is due to contribution of sediment input. Ammonia was observed with more apparent diversity and it decreased gradually from west to east compared with nitrite along the BS transect in the Bering Sea. The Anadyr current and the Alaska Coastal Current have important influence on the concentration of nutrients.

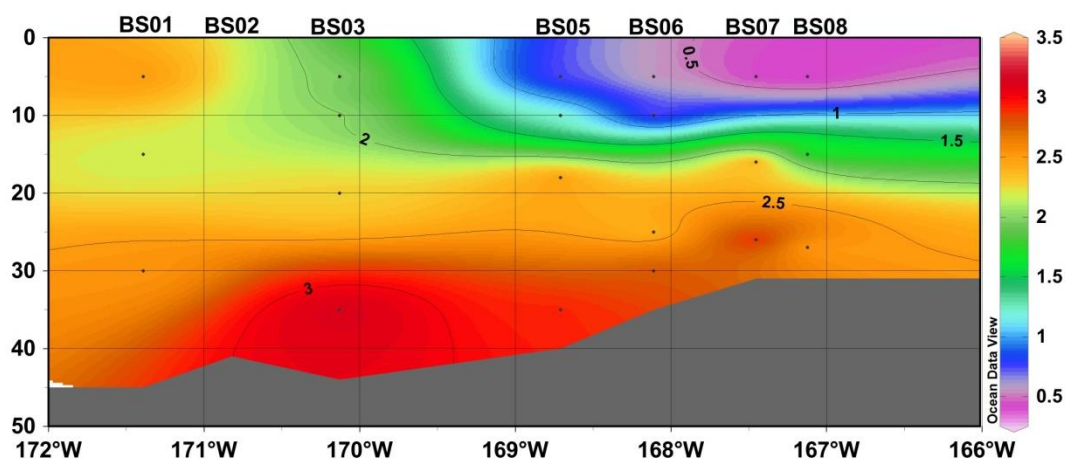


Fig. 5-11 Distribution of ammonia ($\mu\text{mol/L}$) along the BS transect in the Bering Sea

The R transect is located in the Chukchi Sea. Compared to the Bering shelf, nitrite in the water column in the Chukchi Sea has more obvious vertical distribution, with nitrite increase with increasing depth (Fig. 5-12). The highest concentration of nitrite was found in the subsurface water of R04.

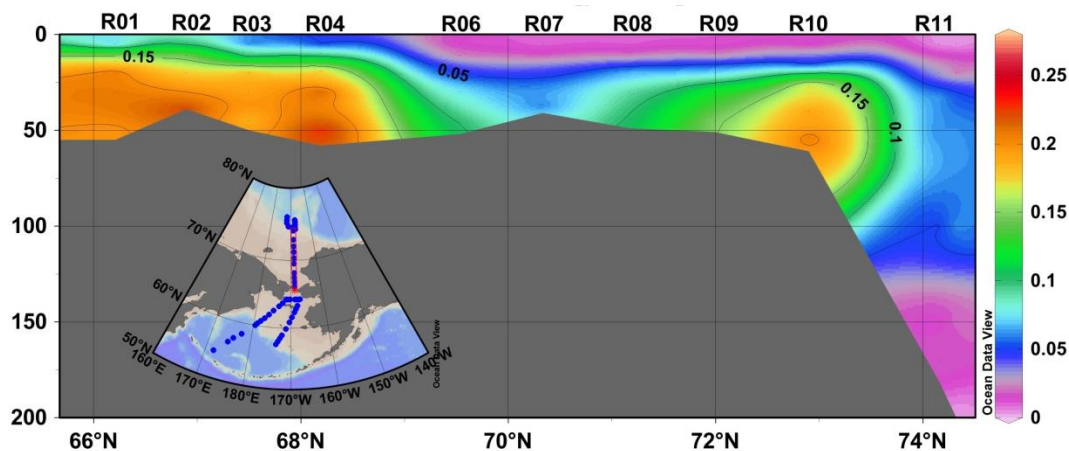


Fig. 5-12 Distribution of nitrite ($\mu\text{mol/L}$) along the R transect in the Chukchi Sea

The distribution of ammonia has a similar pattern with nitrite in the R transect (Fig. 5-13). The high ammonia was usually observed in the bottom water. The highest concentration of ammonia ($6.64 \mu\text{mol/L}$) was found in the bottom water of R09. The concentration of ammonia was gradually dropped at the station of R11.

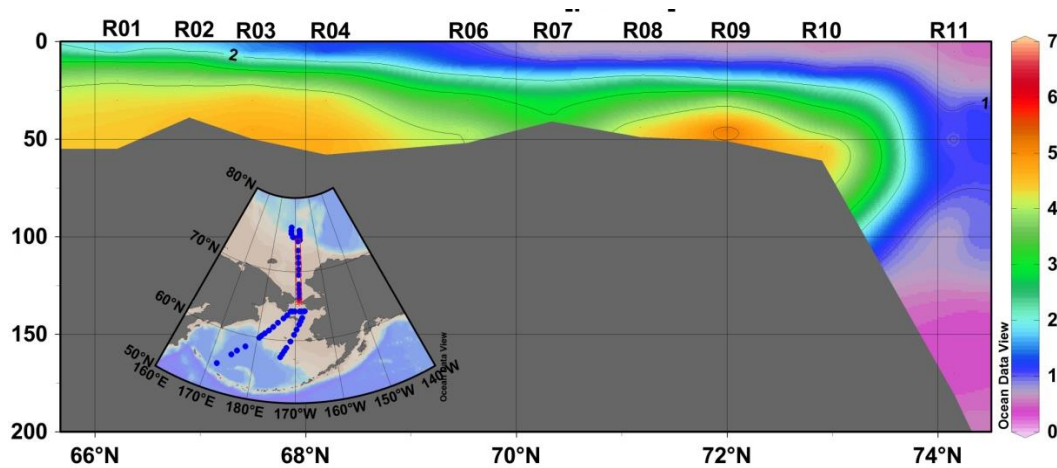


Fig. 5-13 Distribution of ammonia ($\mu\text{mol/L}$) along the R transect in the Chukchi Sea

Dissolved oxygen (DO) was measured during the cruise in September. Fig. 5-14 presented the distribution of DO along the BS transect in the Bering Sea. The average value of DO concentration was $305.3 \mu\text{mol/L}$ in the surface water. DO concentration in surface water was observed with the maximum of $324.8 \mu\text{mol/L}$ at the BS07 station and minimum of $280.2 \mu\text{mol/L}$ at the BS01 station. The average value of DO concentration was $303.0 \mu\text{mol/L}$ in the bottom. DO concentrations was observed with the maximum of $325.5 \mu\text{mol/L}$ and minimum of $281.3 \mu\text{mol/L}$ in bottom water. The changes in oxygen concentration were confined in a small range from surface to bottom at stations BS01, BS02 and BS03 due to vertical mixing.

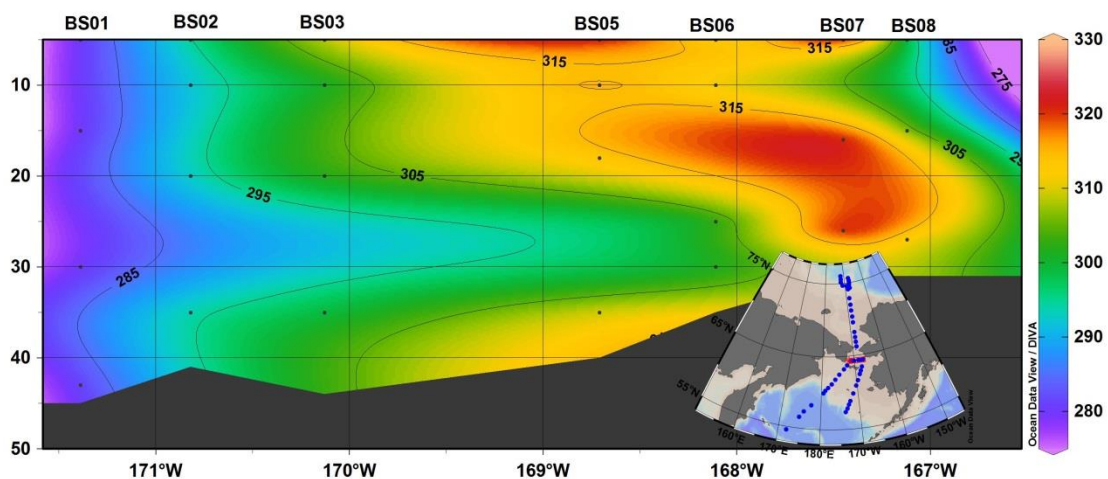


Fig. 5-14 Distribution of oxygen along the BS transect in the Bering Sea

Surface seawater $p\text{CO}_2$ were collected from the underway pumping system at a depth of about 2.5 m during navigation in the U.S. EEZ. During the survey, the study area was completely ice-free. The surface seawater $p\text{CO}_2$ along the cruise track varied between 144 and 648 μatm (Fig. 5-15), with an average value of 339 ± 73 μatm . The highest surface $p\text{CO}_2$ values was found in the western Bering Strait, which was related to the upwelling event, and the lower values were generally observed in the Bering Sea and Chukchi Sea shelf area, which were driven by biological processes. In most areas of the western Arctic Ocean, the seawater $p\text{CO}_2$ was less than the atmospheric $p\text{CO}_2$ level. Thus, despite a small CO_2 out gassing area, the western Arctic Ocean still acted as a net ocean CO_2 sink.

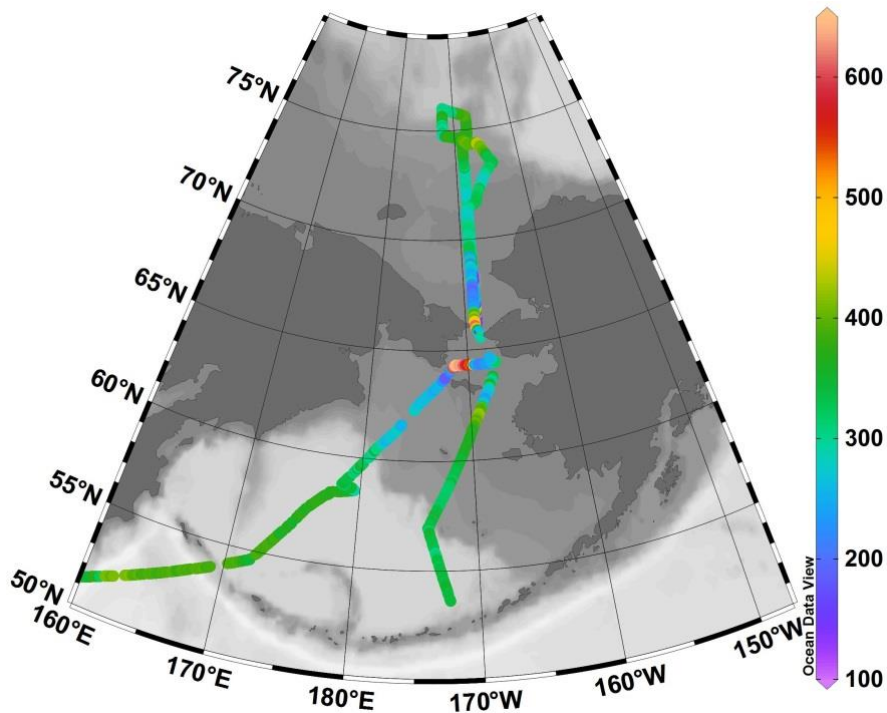


Fig. 5-15 Distributions of surface $p\text{CO}_2$ (μatm) in the study area

Microplastics in surface seawater were sampled by manta trawl, which has the area of $0.8 \text{ m} \times 1.2 \text{ m}$, and towing mesh was $150 \mu\text{m}$. The micro

plastics samples were filtered and stored under -18°C . There were 10 microplastics samples of surface sea water collected by trawling in the shelf of Chukchi and Bering Sea, and Bering Strait in the U.S. EEZ (Fig. 5-16). Some red and green pieces were found in some samples (Fig. 5-17). All filtered samples will be analyzed for count and type of microplastics using an infrared microscope in the lab.

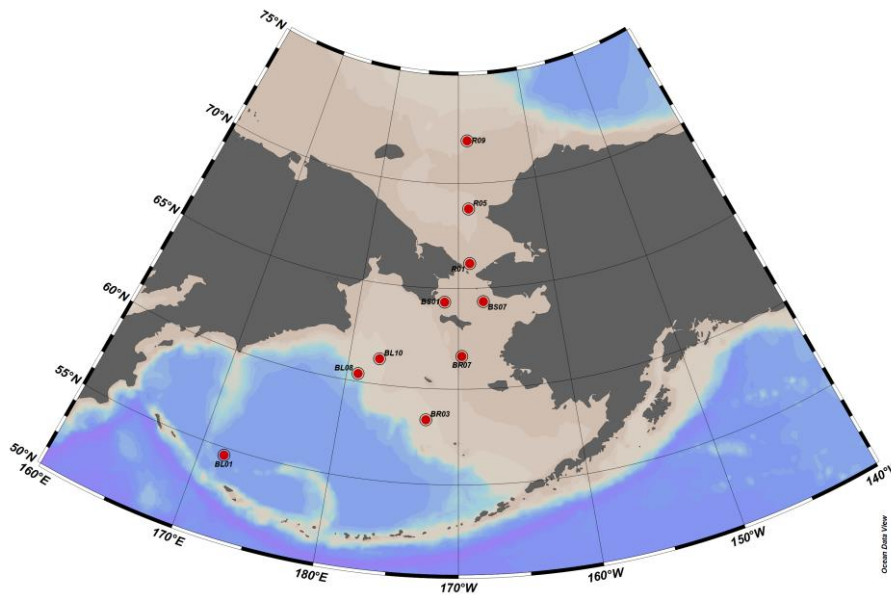


Fig. 5-16 Locations of microplastics samples collected



Fig. 5-17 Microplastics sample of station BR03

5.3 Marine Biology

Coordinator:

Wuchang Zhang

No. 7 Nanhai Road, Qingdao, Shandong, 266071

Institute of Oceanology, Chinese Academy of Sciences

Email: wuchangzhang@qdio.ac.cn

5.3.1 Phytoplankton & Zooplankton net vertical trawling

Zooplankton and phytoplankton samples were taken in 16 stations (Fig. 5-18) by net vertical trawling at a speed of 0.5 m s^{-1} from bottom to surface. Full water column (from 2 m above the bottom to surface) was sampled at stations shallower than 200 m, and only the upper 200 m layer was sampled at deep stations. Immediately after captured, plankton samples were preserved in buffered 5% formalin solution for species identification. To determine community composition and abundance, the formalin-preserved zooplankton samples were processed under a dissecting microscope (Nikon, SMZ645) in the laboratory. A total of 46 species and unspecified taxa were recognized. The net phytoplankton abundance ranged from 6950-733440 cells/L with different dominant genus in different stations.

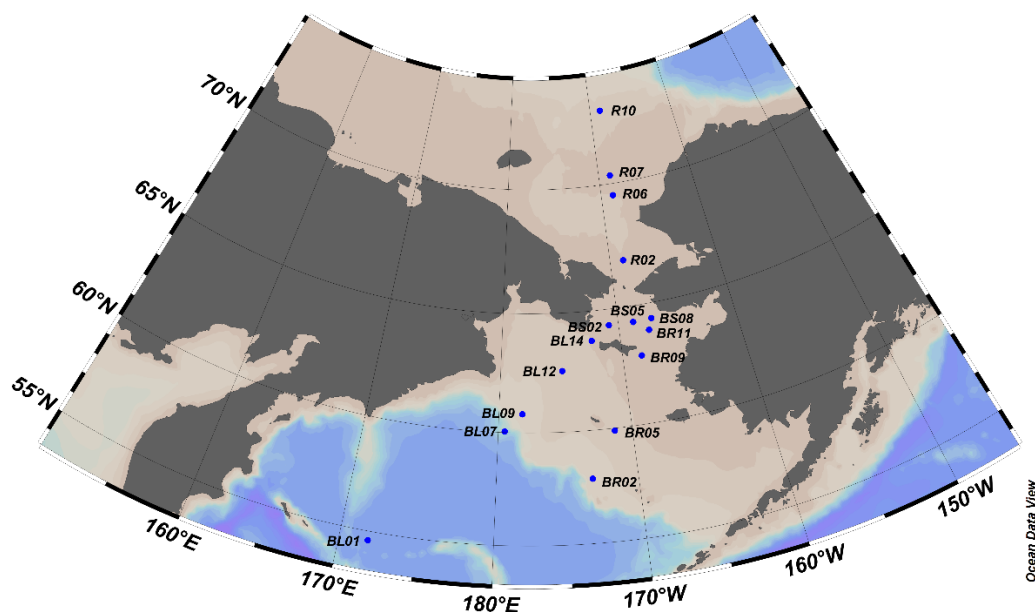


Fig. 5-18 Stations where plankton net vertical trawling were carried out.

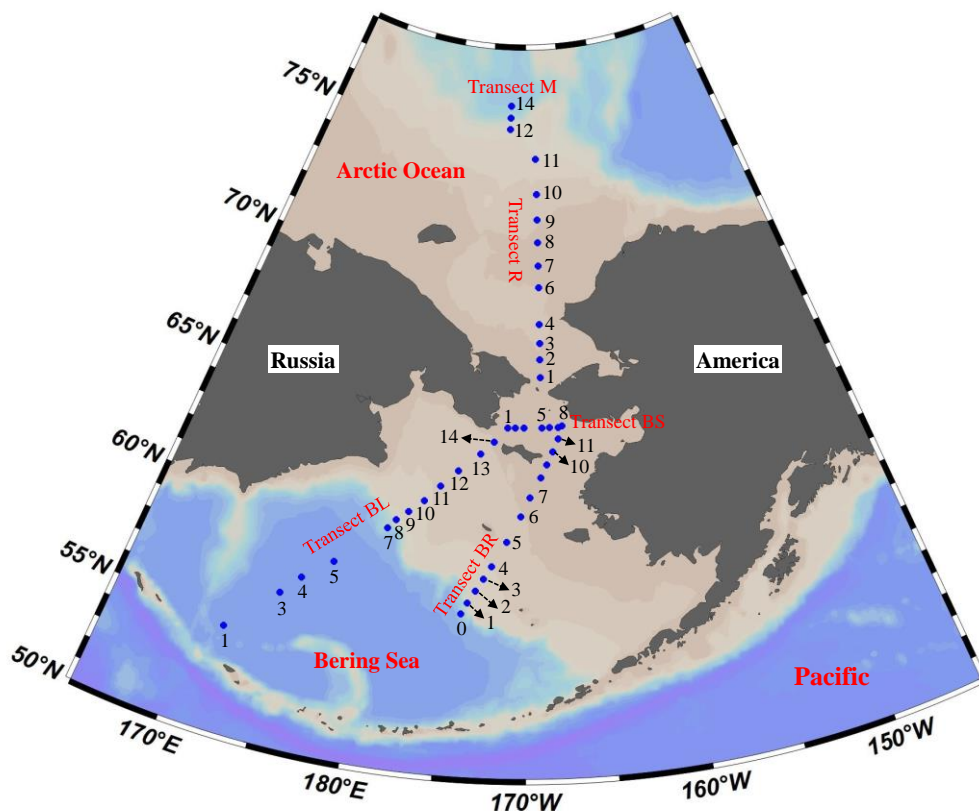


Fig. 5-19 Sample stations of microzooplankton ciliates.

5.3.2 Planktonic ciliate abundance

Samples were obtained from 44 stations (37 of them were in the U.S. EEZ, Fig. 5-19) with sampling layers ranged from surface to 200 m (or the bottom shallower than 200 m, then to bottom).

The vertical distribution and community structure of planktonic ciliates were investigated in the Bering Sea, Bering Strait and the Arctic Ocean. Vertical distribution pattern of planktonic ciliates showed “surface-peak” in three seas. Ciliate abundance ranged from 181-5617 ind/L, 324-9241 ind/L, 453-3415 ind/L and 37-5050 ind/L in the transect BL, BR, BS and R, respectively. For planktonic ciliate community structure, the aloricate ciliate belonged to the dominant group with abundance proportion ranged from 32.2-100% ($87.1 \pm 12.3\%$) in all transects. Ciliate total abundance was high in the shelf area than that of the oceanic areas in the Bering Sea and the Arctic Ocean (Fig. 5-20).

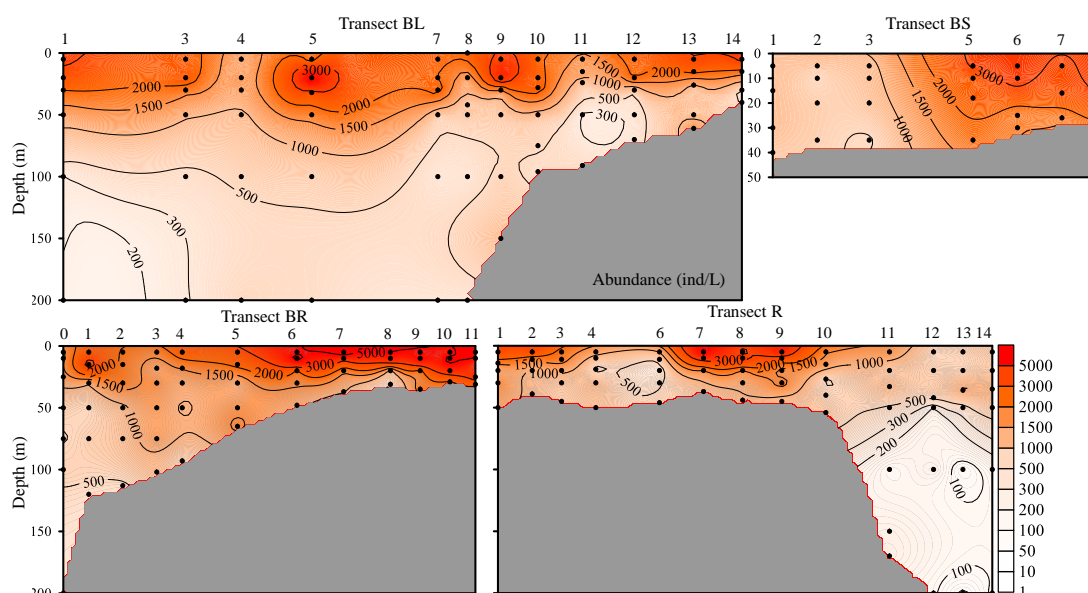


Fig. 5-20 Total abundance of planktonic ciliates along the transects.

5.3.3 Chl a concentration

During the 10th Chinese Arctic Research Expedition, we collected a total of 150 valid samples from 32 stations in the U.S. EEZ for Chlorophyll a (Chl a) concentration analysis. These stations were mainly distributed in 4 transects (BL, BR, BS, R) (Fig. 5-21). The Chl a concentrations ranged from 0~17.75 mg/m³. The highest value was found at the mouth of the Bering Sea. Chl a concentrations were generally

higher in the continental shelves (Bering Sea and Chukchi Sea) than those of deep basins. In the Bering Sea, Chl a concentrations were generally higher on the left side than the right. Vertically, subsurface chlorophyll maximum (SCM) was prominent in deeper stations. In the followings, we detailed the distribution of Chl a in each transect.

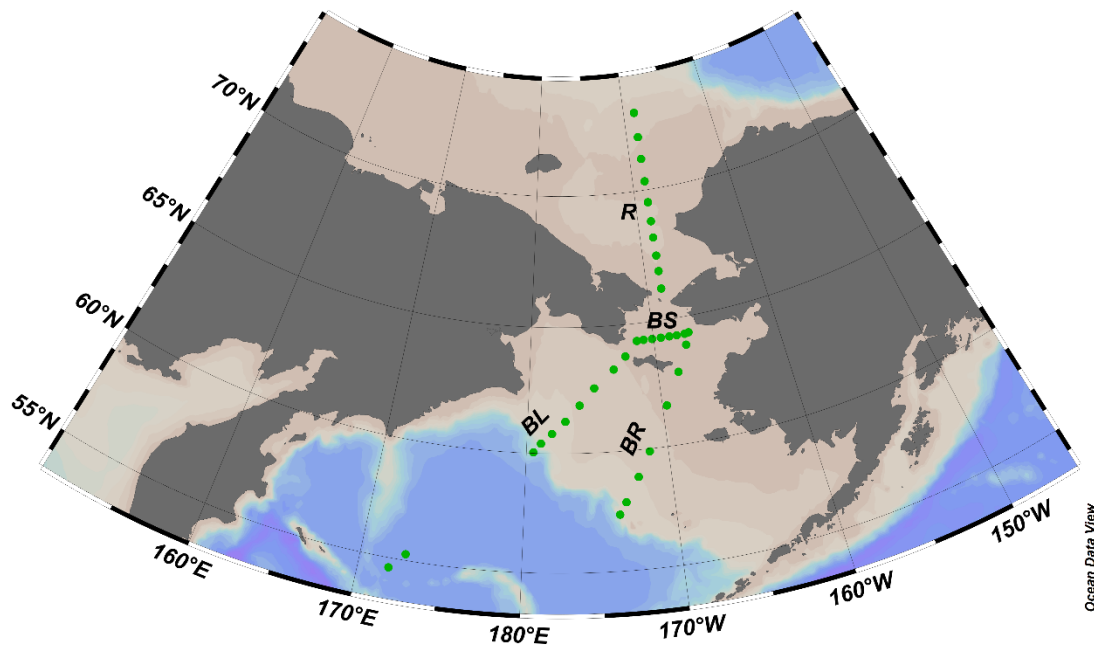


Fig. 5-21 Stations of Chlorophyll a sampling in the Bering Sea and the Chukchi Sea

5.3.4 Bottom trawling

The sampling was conducted using a triangular bottom trawl net (2.2 m width, 0.65 m height, and 6.5 m length; 20 mm mesh size). Bottom trawls for benthos and demersal fish were completed in 14 stations in the U.S. EEZ. Five stations of bottom trawling for benthos and demersal fish were carried out at the Chukchi Sea with the other 9 stations at Bering Sea (Fig. 5-22).

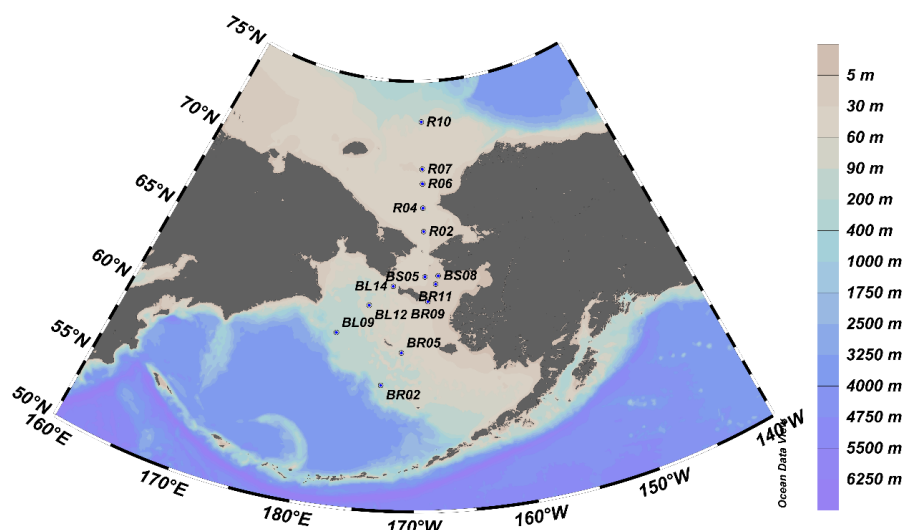


Fig. 5-22 Locations of bottom trawling for benthos and demersal fish

Samples of benthos and demersal fish collected by bottom trawling were both preserved at - 20 °C. All these samples will be examined for species identification.

a. Fish

We conducted benthic trawlings in 14 stations in the U.S. EEZ and captured 17 fish samples in the EEZ of Bering Sea and Chukchi Sea. A total of 5 different species were identified. Basic morphological parameters were also measured (Table 5-1).

Table 5-1 Basic morphological parameters of fish captured in the EEZ of Bering Sea and Chukchi Sea (NA: not applicable)

Station	Species name	Body length (mm)	Full Length (mm)	Body weight (g)
BL09	No fish catch	NA	NA	NA
BL12	No fish catch	NA	NA	NA
BL14	No fish catch	NA	NA	NA
BS05	No fish catch	NA	NA	NA
BS08	<i>Artediellus scaber</i>	70	83	11.1
	<i>Artediellus scaber</i>	67	80	10
	<i>Artediellus scaber</i>	39	45	2
R02	<i>Gymnocanthus</i>	115	134	28.5
	<i>tricuspis</i>			
R04	No fish catch	NA	NA	NA
R06	No fish catch	NA	NA	NA

R07	<i>Gymnocanthus</i>	49	60	2.4
	<i>tricuspis</i>			
	<i>Gymnocanthus</i>	53	63	2.6
	<i>tricuspis</i>			
R10	No fish catch	NA	NA	NA
BR11	<i>Pleuronectes</i>	471	533	2023.5
	<i>quadrituberculatus</i>			
	<i>Pleuronectes</i>	463	523	1890.6
	<i>quadrituberculatus</i>			
	<i>Pleuronectes</i>	244	286	1065.7
	<i>quadrituberculatus</i>			
	<i>Pleuronectes</i>	246	275	953.8
	<i>quadrituberculatus</i>			
	<i>Pleuronectes</i>	233	253	913.1
	<i>quadrituberculatus</i>			
	<i>Pleuronectes</i>	100	112	564.0
	<i>quadrituberculatus</i>			
BR09	<i>Ulcina olrikii</i>	65	70	1.9
BR05	No fish catch	NA	NA	NA
BR02	<i>Boreogadus saida</i>	72	85	3.9
	<i>Boreogadus saida</i>	74	86	3.6
	<i>Boreogadus saida</i>	64	73	2.6
	<i>Boreogadus saida</i>	60	71	2.3

b. Benthos

A total of 86 different taxa were identified in 14 stations of the study area (Table 5-2), of which mollusc was the most abundant, with a total of 41 species, whereas there were 17, 15, 6, 4, 1, 1 and 1 echinoderm, crustacean, polychaetes, bryozoan, chordata, cnidaria and nemertinea species, respectively. The mollusc *Buccinum oedematum* and crustaceans *Chionoecetes opilio* and *Pagurus pubescens* were the most abundant species.

Table 5-2 The list of macrobenthos species in the U.S. EEZ of Chukchi Sea and Bering Sea

Station	Type	mon/day/yr	Species
BL09	trawling	8/28/2019	<i>Serripes laperousii</i> (Deshayes, 1839)
			<i>Musculus niger</i> (J.E. Gray, 1824)
			<i>Ciliatocardium ciliatum</i> (Fabricius, 1780)
			<i>Yoldia limatula</i> (Say, 1831)
			<i>Euspira pallida</i> (Broderip & G. B. Sowerby I, 1829)
			<i>Buccinum cyaneum</i> Bruguière, 1789
			<i>Buccinum micropoma</i> Thorson, 1944
			<i>Buccinum oedematum</i> Dall, 1907
			<i>Buccinum ciliatum</i> (Fabricius, 1780)
			<i>Beringius</i> sp.
			<i>Chionoecetes opilio</i> (O. Fabricius, 1788)
BL12	trawling	8/29/2019	<i>Neptunea</i> sp.
			<i>Buccinum oedematum</i> Dall, 1907
			<i>Buccinum micropoma</i> Thorson, 1944
			<i>Aforia circinata</i> (Dall, 1873)
			<i>Clinopegma hirsutum</i> Tiba, 1971
			<i>Aulacofusus herendeeni</i> (Dall, 1902)
			<i>Latisipho hypolispus</i> (Dall, 1891)
			<i>Serripes groenlandicus</i> (Mohr, 1786)
			<i>Cardiomya behringensis</i> (Leche, 1883)
			<i>Euspira pallida</i> (Broderip & G. B. Sowerby I, 1829)
			<i>Strongylocentrotus</i> sp.
BL14	trawling	8/29/2019	<i>Chionoecetes opilio</i> (O. Fabricius, 1788)
			<i>Argis lar</i> (Owen, 1839)

			<i>Cryptonatica russa</i> (Gould, 1859)
			<i>Ennucula tenuis</i> (Montagu, 1808)
			<i>Modiolus modiolus</i> (Linnaeus, 1758)
			<i>Macoma calcarea</i> (Gmelin, 1791)
			<i>Ophiura sarsii</i> Lütken, 1855
BR11	trawling	9/7/2019	<i>Chionoecetes opilio</i> (O. Fabricius, 1788)
			<i>Pagurus pubescens</i> Krøyer, 1838
			<i>Argis lar</i> (Owen, 1839)
			<i>Neptunea beringiana</i> (Middendorff, 1848)
			<i>Megangulus venulosus</i> (Schrenck, 1861)
			<i>Beringius stimpsoni</i> (Gould, 1860)
			Fascioliariidae und.
			<i>Buccinum micropoma</i> Thorson, 1944
			<i>Serripes laperousii</i> (Deshayes, 1839)
BR09	trawling	9/7/2019	<i>Chionoecetes opilio</i> (O. Fabricius, 1788)
			<i>Hyas ursinus</i> Rathbun, 1924
			<i>Henricia</i> sp.
			<i>Pagurus pubescens</i> Krøyer, 1838
			<i>Neptunea heros</i> (Gray, 1850)
			<i>Buccinum scalariforme</i> Møller, 1842
			<i>Lussivolutopsius furukawai</i> (Oyama, 1951)
			<i>Strongylocentrotus pallidus</i> (G. O. Sars, 1871)
			<i>Flustra</i> sp.
			<i>Eucratea loricata</i> (Linnaeus, 1758)
			<i>Leptasterias</i> (<i>Hexasterias</i>) <i>camtschatica</i> (Brandt, 1835)
			<i>Psolus chitonoides</i> Clark, 1901
			<i>Potamica</i> sp.
BR05	trawling	9/8/2019	Buccinidae und.
			<i>Boltenia ovifera</i> (Linnaeus, 1767)
			<i>Chionoecetes opilio</i> (O. Fabricius, 1788)
			<i>Leptasterius</i> sp.
			<i>Psolus</i> sp.
BR02	trawling	9/8/2019	Actiniidae und.
			<i>Gersemia rubiformis</i> (Ehrenberg, 1834)
			Terebrillidae und.
			<i>Gorgonocephalus</i> sp.
			<i>Ocnus glacialis</i> (Ljungman, 1879)
R10	trawling	9/1/2019	<i>Ctenodiscus crispatus</i> (Bruzeliuss, 1805)
			<i>Urasterias lincki</i> (Müller & Troschel, 1842)
			<i>Ophiura sarsii</i> Lütken, 1855
			<i>Gorgonocephalus arcticus</i> Leach, 1819
			<i>Chionoecetes opilio</i> (O. Fabricius, 1788)
			<i>Pagurus pubescens</i> Krøyer, 1838

			<i>Eualus belcheri</i> (Bell, 1855)
			<i>Pandalus borealis</i> Krøyer, 1838
			<i>Eualus gaimardii</i> (H. Milne Edwards, 1837)
			<i>Yoldia limatula</i> (Say, 1831)
			<i>Neptunea heros</i> (Gray, 1850)
			<i>Cryptonatica russa</i> (Gould, 1859)
			<i>Macoma calcarea</i> (Gmelin, 1791)
			<i>Cyclocardia crebricostata</i> (A. Krause, 1885)
R07	trawling	8/31/2019	<i>Psolus chitonoides</i> Clark, 1901
			<i>Amicula vestita</i> (Broderip & G. B. Sowerby I, 1829)
			<i>Hyas coarctatus</i> Leach, 1815
			<i>Buccinum oedematum</i> Dall, 1907
			<i>Beringius behringii</i> (Middendorff, 1848)
			<i>Buccinum scalariforme</i> Møller, 1842
			<i>Neptunea heros</i> (Gray, 1850)
			<i>Asterias</i> sp.
			<i>Crossaster papposus</i> (Linnaeus, 1767)
			<i>Gersemia rubiformis</i> (Ehrenberg, 1834)
			<i>Alcyna</i> sp.
			<i>Chionoecetes opilio</i> (O. Fabricius, 1788)
			Actiniidae und.
			Amphipoda und.
			<i>Ophiura sarsii</i> Lütken, 1855
			<i>Argis lar</i> (Owen, 1839)
			<i>Argis hozawai</i> (Yokoya, 1939)
			<i>Securiflustra securifrons</i> (Pallas, 1766)
			<i>Eucratea loricata cornuta</i> Osburn, 1932
			<i>Sclerocrangon boreas</i> (Phipps, 1774)
			<i>Pandalus borealis</i> Krøyer, 1838
			<i>Eualus zarenkovi</i> Komai & De Grave, 2015
			<i>Eualus belcheri</i> (Bell, 1855)
			<i>Lebbeus polaris</i> (Sabine, 1824)
			<i>Spirontocaris spinus</i> (Sowerby, 1805)
R06	trawling	8/31/2019	<i>Pagurus pubescens</i> Krøyer, 1838
			<i>Chionoecetes opilio</i> (O. Fabricius, 1788)
			<i>Leptasterias polaris acervata</i> (Stimpson, 1861)
			<i>Ciliatocardium ciliatum</i> (Fabricius, 1780)
			<i>Yoldia limatula</i> (Say, 1831)
			<i>Melongenidae</i> sp.
			<i>Latisipho hypolispus</i> (Dall, 1891)
			<i>Neptunea heros</i> (Gray, 1850)
			<i>Argis lar</i> (Owen, 1839)
			<i>Pandalus borealis</i> Krøyer, 1838

			Actiniidae und.
			<i>Nephtys</i> sp.
			<i>Nephtys paradoxa</i> Malm, 1874
			<i>Eunoe depressa</i> Moore, 1905
R04	trawling	8/31/2019	<i>Ampharete acutifrons</i> (Grube, 1860)
			<i>Buccinum middendorffii</i> Verkrüzen, 1882
			<i>Buccinum micropoma</i> Thorson, 1944
			<i>Serripes groenlandicus</i> (Mohr, 1786)
			<i>Pandalus borealis</i> Krøyer, 1838
			<i>Argis lar</i> (Owen, 1839)
			<i>Onchidoris</i> sp.
			Actiniidae und.
R02	trawling	8/30/2019	<i>Neptunea beringiana</i> (Middendorff, 1848)
			<i>Neptunea vinosa</i> (Dall, 1919)
			<i>Chlamys behringiana</i> (Middendorff, 1849)
			<i>Gorgonocephalus arcticus</i> Leach, 1819
			<i>Asterias rubens</i> Linnaeus, 1758
			<i>Paralithodes camtschaticus</i> (Tilesius, 1815)
			<i>Pagurus pubescens</i> Krøyer, 1838
			<i>Buccinum maltzani</i> Pfeffer, 1886
			<i>Cryptonatica russa</i> (Gould, 1859)
			<i>Buccinum micropoma</i> Thorson, 1944
			Eteoninae und.
			Nemertinea und.
			<i>Chionoecetes opilio</i> (O. Fabricius, 1788)
			<i>Pandalus borealis</i> Krøyer, 1838
			<i>Neptunea beringiana</i> (Middendorff, 1848)
			<i>Buccinum middendorffii</i> Verkrüzen, 1882
			<i>Crossaster papposus</i> (Linnaeus, 1767)
			<i>Strongylocentrotus pallidus</i> (Sars G.O., 1872)
			<i>Ampharete acutifrons</i> (Grube, 1860)
BS05	trawling	8/29/2020	<i>Chionoecetes opilio</i> (O. Fabricius, 1788)
			<i>Gersemia rubiformis</i> (Ehrenberg, 1834)
			<i>Beringius behringii</i> (Middendorff, 1848)
			<i>Pandalus borealis</i> Krøyer, 1838
			<i>Spirontocaris spinus</i> (Sowerby, 1805)
BS08	trawling	8/29/2019	Buccinidae Rafinesque, 1815
			<i>Boltenia ovifera</i> (Linnaeus, 1767)
			<i>Chionoecetes opilio</i> (O. Fabricius, 1788)
			<i>Leptasterius</i> sp.
			<i>Psolus</i> sp.

c. Microplastic contamination in benthic organisms

The 10th Chinese National Arctic Research Expedition (10th CHINARE-Arctic) investigated microplastic (MP) contamination in benthic organisms from 7 stations in the U.S. EEZ (Fig. 5-23),.

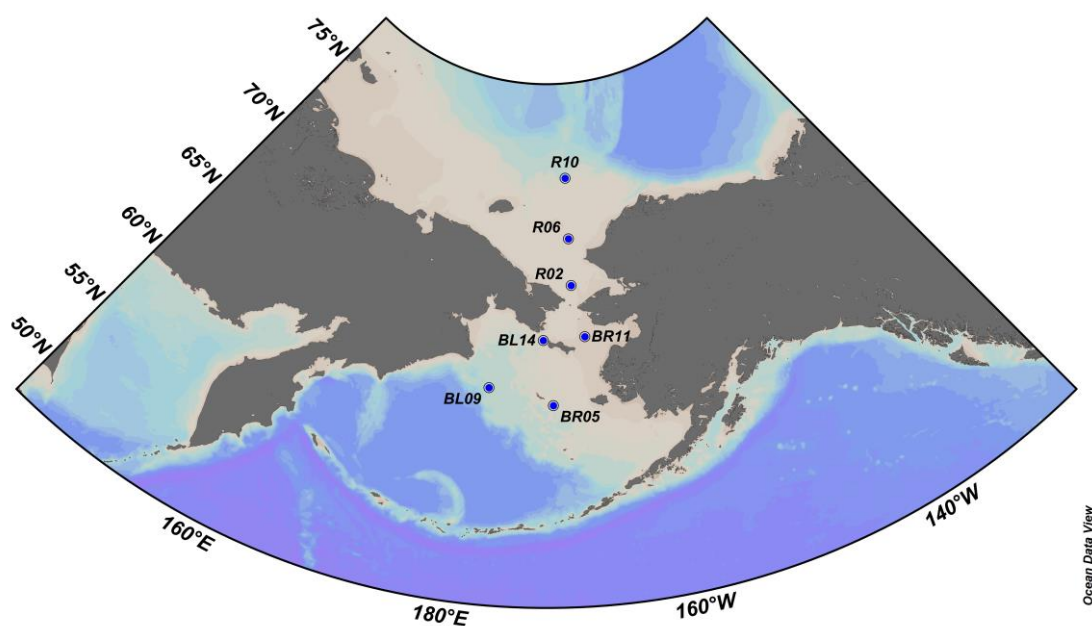


Fig. 5-23 Sampling locations for microplastics in benthic organisms

The proportions of positive individuals ranged from 20% to 80% and the abundances of MPs in the benthic organisms ranged from 0.27 to 4.24 items/individual with the mean of 1.72 items/individual, which was relatively higher than those in the benthic organisms reported by our previous expeditions. The benthic organisms from high latitude areas ingested obviously higher MP abundances than those from low latitude areas, indicating the melting sea ice may contribute to the MP accumulation in the benthos. The predator organisms such as snow crab (*Chionoecetes opilio*), starfish (*Asterias rubens*) and demersal fish

(*Gymnocanthus tricuspis*) ingested higher quantities of MPs, suggesting that the trophic transfer of MPs through benthic food webs may play a critical role. The snow crab could function as a bioindicator of MP pollution in the Arctic due to its wide distribution and could reflect the spatial variability in MP contamination. The predominant types and compositions of MPs in the benthic organisms were fiber, polyester (PES) and polyamide (PA), indicating clothing and textile fibers as well as “ghost fishing gear” may be important sources of MPs in this area. Scanning electron microscopy (SEM) showed that the surface morphology of MPs in benthic organisms from Arctic was rougher and more weathered than those in coastal organisms, indicating the possibility of long-distance migration.

5.3.5 Benthos Clamshell grab sampling

Macrobenthos samples in five stations (BL10, BL13, R01, R05 and R08, Table 5-3) in U.S. EEZ were taken by DDC-2 Box-corer. Each sample was rinsed through 0.5 mm mesh sieves, and the residue containing the benthic Macro fauna was fixed in 70% ethanol. The most species of macrobenthos are polychaeta. The species composition, abundance and biomass will be sorted, identified and calculated in lab in the future.

Table 5-3 the information of macrobenthos sampling

Station	longitude	Latitude	Depth	Description
BL10	177°14.3982'W	61°17.1501'N	118m	Mollusca, brittle star, polychaeta

BL13	173°26.200'W	63°17.399'N	66m	Polychaeta
R01	168°45.1101'W	66°12.6361'N	55m	Polychaeta, brittle star, Hermit crabs
R05	168°44.7248'W	68°48.3726'N	55m	Small brittle star, Mollusca, polychaeta
R08	168°45.1531'W	71°10.3928'N	49m	Amphipoda, brittle star, polychaeta

5.4 Marine Geology

Coordinator:

Zhihua Chen

No.6 Xianxialing Road, Qingdao, Shandong, 266061

The First Institute of Oceanography,

Ministry of Natural Resources

Email: chenzia@fio.org.cn

Overall, twenty-eight stations of surface sediment and one gravity core were collected in the Chukchi and Bering seas by the tenth Chinese Arctic Research Expedition (Fig. 5-24).

5.4.1 Surface sediments

The grain size compositions and mean size of surface sediments are shown in Table 5-4 and Fig. 5-25. In general, surface sediments on the continental shelf of the Chukchi and Bering seas consist of sandy silt or silty sand with mean grain size of 2.91~6.22 ϕ . The varieties of sediment types and compositions in the study area are caused by both regional special features of bottom relief and hydrodynamic particularities in the Bering and Chukchi seas.

The gravel-pebble badly sorted sediments with noticeable admixture of coarse-grained sand prevail in the area near the Bering Strait (BL14, BR09). Sediments on the western continental shelf side of the Bering Sea are relatively fine and rich in mud (silt and clay) especially near the Anadyr Gulf (BL10, BL11, BL12, BL13). On the eastern side of the Bering Sea, sediments contain both mud and gravel near Saint Laurence

Island (BR09). Sediments contain more silt and fine sand southward on the middle shelf (BR05, BR04) and then become coarser and fine-sand dominated on the outer shelf and continental slope (BR01, BR00), indicating local changes in sediment sources especially from the Yukon River and current's impacts on sediment transport, deposition and reworking.

A wide variety of sediment types are observed in surface sediments of the Chukchi Sea. Along the meridian line of 170°W in the Chukchi Sea, sediments near the Bering Strait contain some rock clasts (R01); sediments become finer and clay-rich near the Kotzebue Bay (R03), coarser in the central channel (R04) and on the Herald Shoal (R07), and then finer on the outer shelf (R08, R09, R10). In general, relatively high productivity results in the development of diatom-bearing silts in the central (deep-water) part of the Chukchi Sea (R03, R09, R10).

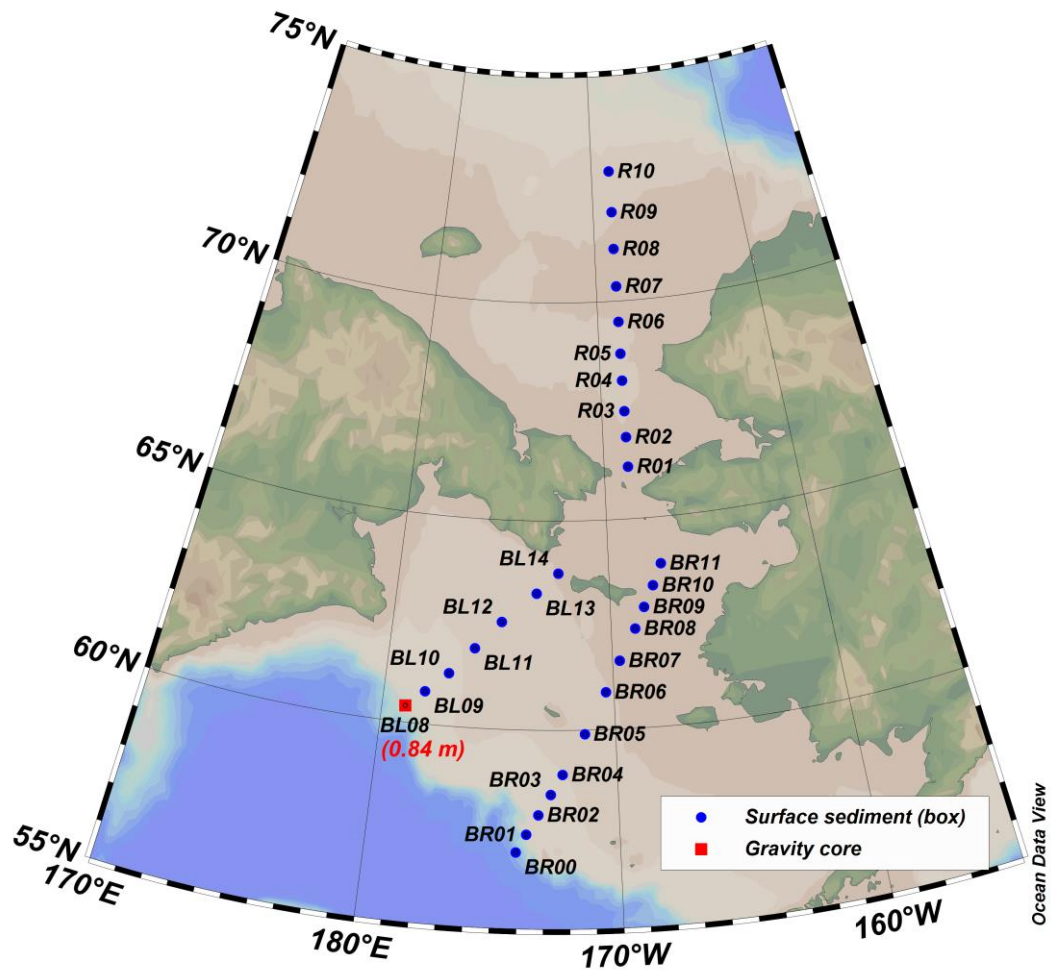


Fig. 5-24 Surface sediments and cores collected in the Bering and Chukchi seas

Table 5-4 Grain size compositions of surface sediments in the Bering and Chukchi seas

No.	Station	Longitude (°W)	Latitude (°N)	Water depth (m)	Gravel (%)	Sand (%)	Silt (%)	Clay (%)	Folk's nomenclature	Area
1	BL08	179.0013	60.3992	505.4	0.00	50.94	43.77	5.29	Silty sand	Bering Sea
2	BL09	178.2111	60.7973	157.0	0.00	29.49	65.11	5.40	Sandy silt	
3	BL10	177.2399	61.2857	118.0	0.00	20.15	70.86	8.99	Sandy silt	
4	BL11	176.1754	61.9258	98.0	0.00	8.53	80.41	11.06	Silt	
5	BL12	175.0103	62.5934	71.0	0.00	21.98	68.69	9.32	Sandy silt	
6	BL13	173.4367	63.29	66.7	0.00	17.60	74.63	7.78	Sandy silt	
7	BL14	172.4077	63.7666	44.3	3.00	72.24	22.67	2.09	Silty sand	
8	R01	168.7527	66.2106	55.0	2.42	64.14	28.14	5.30	Silty sand	Chukchi Sea
9	R02	168.7482	66.8942	43.3	0.00	40.00	52.56	7.44	Sandy silt	
10	R03	168.7498	67.4948	50.0	0.00	19.46	69.50	11.04	Sandy silt	
11	R04	168.7606	68.1927	57.0	0.00	31.69	60.18	8.13	Sandy silt	
12	R05	168.7473	68.8062	55.0	0.00	14.82	76.51	8.67	Sandy silt	
13	R06	168.7512	69.5333	51.0	0.00	14.49	73.66	11.84	Sandy silt	
14	R07	168.7503	70.3332	41.0	0.00	60.91	31.76	7.33	Silty sand	
15	R08	168.7545	71.1732	49.0	0.00	16.00	75.44	8.56	Sandy silt	

No.	Station	Longitude (°W)	Latitude (°N)	Water depth (m)	Gravel (%)	Sand (%)	Silt (%)	Clay (%)	Folk's nomenclature	Area
16	R09	168.7373	71.9933	51.4	0.00	10.13	77.53	12.34	Sandy silt	Bering Sea
17	R10	168.7448	72.8982	61.1	0.00	10.44	75.37	14.19	Sandy silt	
18	BR11	167.4781	63.9011	35.0	0.00	57.50	38.07	4.43	Silty sand	
19	BR10	167.9389	63.4013	35.0	0.00	62.88	32.70	4.42	Silty sand	
20	BR09	168.4268	62.9067	40.0	0.00	80.51	17.37	2.12	Silty sand	
21	BR08	168.8968	62.4053	35.0	0.00	61.90	33.14	4.96	Silty sand	
22	BR07	169.6772	61.653	43.0	0.00	43.77	52.74	3.49	Sandy silt	
23	BR06	170.3536	60.9051	52.0	0.00	40.10	55.87	4.03	Sandy silt	
24	BR05	171.3069	59.8991	71.0	0.00	28.82	64.99	6.19	Sandy silt	
25	BR04	172.2544	58.9074	98.0	0.00	22.19	71.15	6.66	Sandy silt	
26	BR03	172.7352	58.4049	107.0	0.00	33.32	61.47	5.21	Sandy silt	
27	BR02	173.2263	57.9018	118.0	0.00	43.19	52.70	4.11	Sandy silt	
28	BR01	173.6983	57.405	134.0	0.00	55.90	41.08	3.02	Silty sand	
29	BR00	174.0913	56.9533	1684.0	0.00	53.34	42.88	3.78	Silty sand	

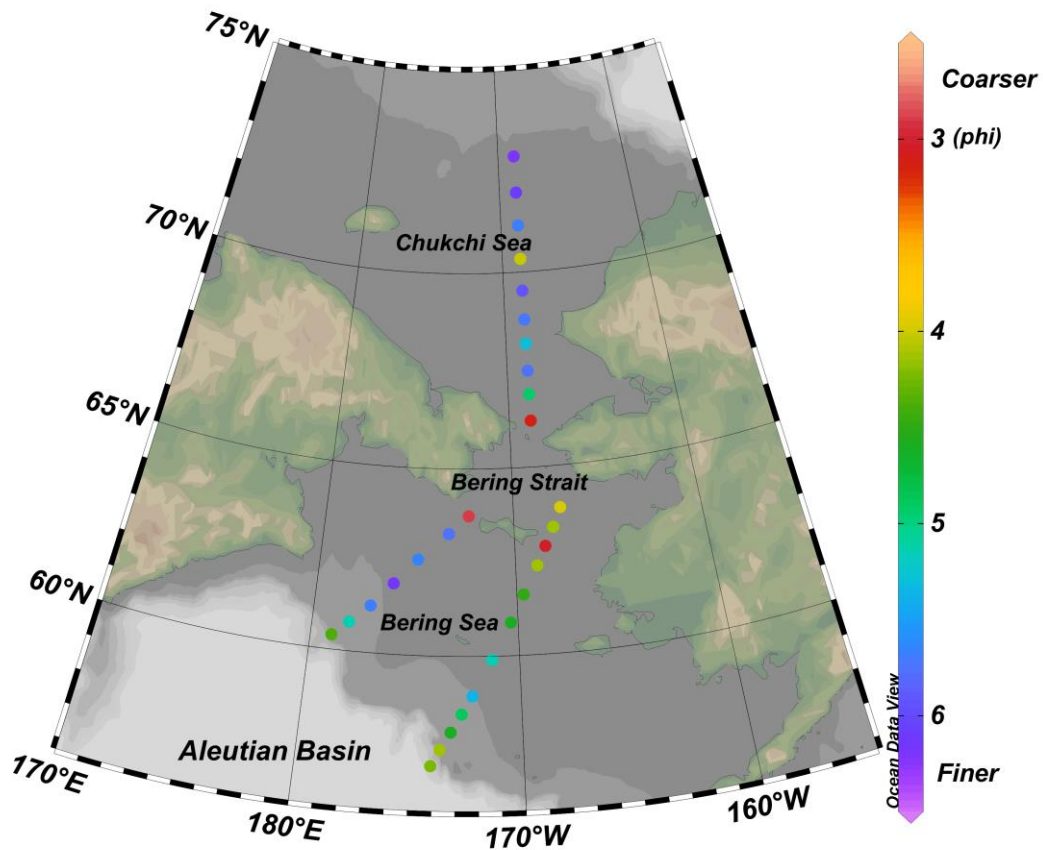


Fig. 5-25 Mean grain size of surface sediments in the Bering and Chukchi seas (ϕ)

5.4.2 Core sediments

For Core BL08 collected on the northwestern continental slope of the Bering Sea (water depth of 505.4 m), sediments are mainly composed of silt (43.77%~62.06%) and sand (29.29%~50.94%) with a little clay (3.38%~8.65%) (Table 5-5).

As shown in Fig. 5-26, Core BL08 can be subdivided into 4 sections. The top section (0~7 cm) is composed of gray silty sand to sandy silt. Section 2 (7~43 cm) is composed mainly of grayish to greenish sandy silt with gradual coarsening trend downwards. Section 3 (43~67 cm) is relatively coarser and contains more sand fraction. Section 4 (67~78 cm) is composed of grayish sandy silt and relatively fine. High-resolution study of sediment cores in the Bering Sea can present records to reveal paleoceanographic changes and the ice-rafted detritus events during Late Quaternary, but Core BL08 is too short to reflect long-term paleoenvironmental changes.

Table 5-5 Grain size compositions of Core BL08 collected in the Bering Sea

No.	Depth (cm)	Gravel (%)	Sand (%)	Silt (%)	Clay (%)	Folk's nomenclature
1	0-2	0.00	50.94	43.77	5.29	Silty sand
2	2-4	0.00	35.12	56.71	8.16	Sandy silt
3	4-6	0.00	35.17	57.80	7.03	Sandy silt
4	6-8	0.00	29.29	62.06	8.65	Sandy silt
5	8-10	0.00	30.43	61.49	8.08	Sandy silt
6	10-12	0.00	33.07	59.37	7.56	Sandy silt
7	12-14	0.00	38.61	54.97	6.42	Sandy silt
8	14-16	0.00	39.99	54.81	5.20	Sandy silt
9	16-18	0.00	33.55	59.28	7.17	Sandy silt
10	18-20	0.00	35.23	57.83	6.94	Sandy silt
11	20-22	0.00	34.34	58.80	6.86	Sandy silt
12	22-24	0.00	37.60	56.02	6.38	Sandy silt
13	24-26	0.00	34.63	57.63	7.74	Sandy silt
14	26-28	0.00	41.15	53.05	5.79	Sandy silt
15	28-30	0.00	35.86	57.36	6.78	Sandy silt
16	30-32	0.00	37.42	56.99	5.58	Sandy silt

No.	Depth (cm)	Gravel (%)	Sand (%)	Silt (%)	Clay (%)	Folk's nomenclature
17	32-34	0.00	36.20	57.18	6.61	Sandy silt
18	34-36	0.00	45.26	49.15	5.59	Sandy silt
19	36-38	0.00	46.30	48.31	5.39	Sandy silt
20	38-40	0.00	36.11	57.95	5.94	Sandy silt
21	40-42	0.00	46.93	48.32	4.74	Sandy silt
22	42-44	0.00	49.76	46.86	3.38	Sandy silt
23	44-46	0.00	50.14	46.32	3.54	Silty sand
24	46-48	0.00	50.11	46.27	3.62	Silty sand
25	48-50	0.00	48.05	48.04	3.90	Sandy silt
26	50-52	0.00	47.28	48.53	4.19	Sandy silt
27	52-54	0.00	48.89	46.73	4.38	Sandy silt
28	54-56	0.00	48.91	47.05	4.03	Sandy silt
29	56-58	0.00	50.08	46.18	3.73	Silty sand
30	58-60	0.00	47.57	48.30	4.13	Sandy silt
31	60-62	0.00	43.59	51.67	4.74	Sandy silt
32	62-64	0.00	48.90	47.45	3.64	Sandy silt
33	64-66	0.00	41.24	53.55	5.20	Sandy silt
34	66-68	0.00	40.30	55.22	4.48	Sandy silt
35	68-70	0.00	34.98	58.94	6.08	Sandy silt
36	70-72	0.00	32.56	61.63	5.81	Sandy silt
37	72-74	0.00	36.22	57.88	5.90	Sandy silt
38	74-76	0.00	38.46	55.99	5.55	Sandy silt
39	76-78	0.00	35.61	58.88	5.51	Sandy silt

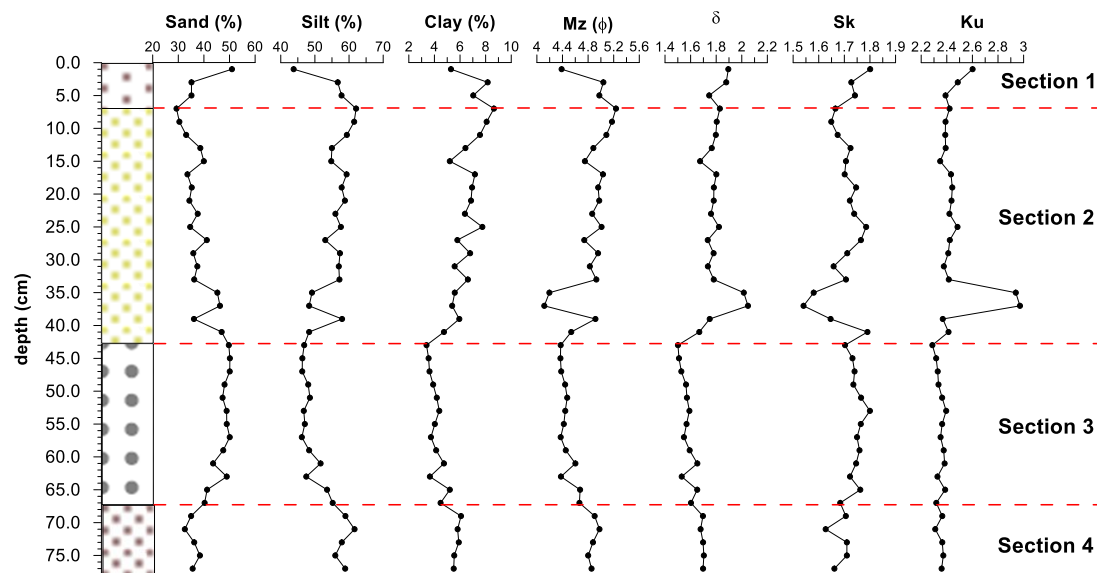


Fig. 5-26 Grain size compositions and parameters of sediments in Core BL08 in the Bering Sea

6. Data submission

According to the above field works in the in the U.S. EEZ during the 10th CHINARE, we summarize the observation data according to disciplines and observation device and/or parameters, and submit it together with this report. Table 6-1 summarizes the data information.

Table 6-1 Data collected from the U.S. EEZ during the 10th CHINARE

Disciplines	Device	Parameters	Number of stations	Number of samples	Number of data files
Meteorology	Vessel-mounted automatic weather station	Wind, air temperature, humidity, air pressure, visibility	9 days (8.24, 8.25, 8.28, 8.29, 8.30, 8.31, 9.1, 9.7, 9.8)	N/A	1
Physical oceanography	Vessel-mounted CT	Surface temperature and salinity	7 days (8.24, 8.25, 8.28, 8.2, 8.30, 8.31, 9.1)	N/A	7
Physical oceanography	CTD and rosette sampler system, Lowered-ADC P, SVP	Temperature, salinity, pressure, current velocity, sound speed	40	120	120
Marine chemistry	Automatic nutrients analyze, dissolved oxygen analyze, pCO ₂ underway system, microscop	Nitrate+Phosphate+Silicate, Nitrite, Ammonium, Dissolved oxygen, pCO ₂ , Microplastics	40 40 38 35 8 days (8.24, 8.28, 8.29, 8.30, 8.31, 9.1, 9.7, 9.8) 10	234 232 206 177 N/A 10	4
Marine ecology	Zooplankton net Phytoplankton net CTD rosette	Zooplankton phytoplankton Chlorophyll a, planktonic ciliate, Benthos by bottom	16 16 32 37 14	16 16 150 178 14	8

	sampler	trawling,	14	14	
	CTD rosette	Fish by bottom	14	14	
	sampler	trawling	5	5	
	Bottom trawler	Microplastics in			
	Bottom trawler	benthos			
	Bottom trawler	Benthos by grab			
	Grab sampler	sampling			
Marine geology	Mastersizer 2000	Grain size of sediment	28 surface sediments, 1 core	67 (28+39)	1

7. Highlights of research results

7.1 Vertical distribution of nutrient tracers in the western Arctic

To understand and explain the nutrient tracer signals in the western Arctic Ocean, the water column was divided into seven layers on the basis of results. The specific characteristics of physical properties and nutrient tracers in the seven water layers are summarized.

Layer I (FL) has the lowest nitrate and silicate concentrations in the water column (means of 0.3 and 2.1 $\mu\text{mol/L}$, respectively), as well as the lowest $\text{NO}_3^-/\text{PO}_4^{3-}$ and $\text{SiO}_3^{2-}/\text{PO}_4^{3-}$ values (means of 0.5 and 2.8, respectively). These low concentrations represent nitrate limitation for algae growth and an excess of phosphate relative to nitrate and silicate. ACW and sBSW are the main components of layer II, which is also known as summer Pacific halocline water. The distribution of ACW and sBSW can be distinguished by a temperature maximum under different salinity ranges.

The upper boundary of layer III (wBSW) can be defined using phosphate ($\text{PO}_4^{3-} > 1.4 \mu\text{mol/L}$) and silicate ($\text{SiO}_3^{2-} > 20 \mu\text{mol/L}$) concentrations. The lower boundary of layer III is defined as an NO/PO value of < 0.85 . Layer III also has the highest concentration of phosphate (mean of 1.67 $\mu\text{mol/L}$) and silicate (mean of 28.2 $\mu\text{mol/L}$), constituting a nutrient maximum in the Canada Basin. The wBSW has the most negative N^* value (mean of $-11.7 \mu\text{mol/L}$) in the water column, followed by sBSW and ACW (mean of $-10.5 \mu\text{mol/L}$). These patterns are controlled by strong denitrification in the Bering-Chukchi Shelf.

Layer IV (AW) is characterized by $0.85 < \text{NO/PO} < 0.90$ and $\text{Si}^* > 4$. Layer V is the thermocline layer. Layer VI (AL) has a thickness of ~ 800 m and originates from the Fram Strait branch. The mean values of

$\text{NO}_3^-/\text{PO}_4^{3-}$, N^* and Si^* are 13.1, 0.8 and $-5.4 \mu\text{mol/L}$, respectively. The difference in N^* ($12.5 \mu\text{mol/L}$) and Si^* ($22.1 \mu\text{mol/L}$) between AL and wBSW is significant. ADW is located in the bottom of the basin (layer VII) and has similar N^* and $\text{NO}_3^-/\text{PO}_4^{3-}$ values to those of AL but higher SiO_3^{2-} and $\text{SiO}_3^{2-}/\text{PO}_4^{3-}$. The chemical signatures of water masses with multiple sources are different. The differences in N^* and Si^* between water layers in the western Arctic Ocean indicate that nutrients can trace and distinguish Pacific and Atlantic waters.

North Atlantic water has the lowest silicate concentration and strong nitrogen fixation in the global oceans. Therefore, water masses originating from the Atlantic Ocean have positive N^* , negative Si^* , and high $\text{NO}_3^-/\text{PO}_4^{3-}$ values. ADW has a nutrient signature similar to that of Atlantic water, except that it has relatively high SiO_3^{2-} concentrations and $\text{SiO}_3^{2-}/\text{PO}_4^{3-}$ values, probably as a result of dissolution of biogenic silica in the deep ocean. AW in the lower halocline has a nutrient signature closer to that of a Pacific source rather than an Atlantic source, as AW originates from the Barents Sea and is chemically transformed through the broad shelf.

Pacific waters in the western Arctic Ocean include the ACW, sBSW, and wBSW, and they dominantly determine the composition of halocline water. The very negative N^* values in these waters indicate dominant nitrogen loss relative to phosphate. These patterns are a consequence of Pacific water being originally nitrate deficient, and there is strong denitrification in the Bering-Chukchi Shelf. The Bering-Chukchi Shelf has active biogeochemical cycles and pelagic production under retreating Arctic sea ice, which enhances the effect of denitrification. The high Si^*

value of wBSW is due to low biological uptake of silicate in winter. The surface inventory of nitrate in FL is low, resulting in nitrogen limitation and low phytoplankton growth in the western Arctic Ocean.

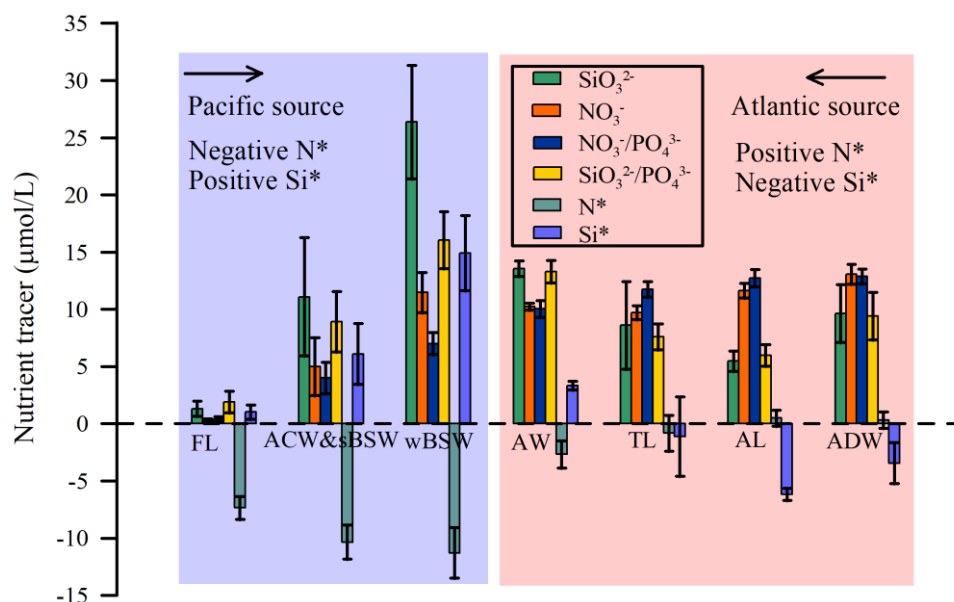


Fig. 7-1. Nutrient tracer plots for each water mass in the western Arctic Ocean.

The vertical distribution of nutrient tracers in the western Arctic Ocean indicates that the surface FL has the lowest nitrate and silicate concentrations in the water column (means of 0.3 and 2.1 $\mu\text{mol/L}$, respectively), as well as the lowest $\text{NO}_3^-/\text{PO}_4^{3-}$ and $\text{SiO}_3^{2-}/\text{PO}_4^{3-}$ values (means of 0.5 and 2.8, respectively). This causes the FL to be nitrate limited, thus inhibiting algae growth. The wBSW has the highest mean concentration of phosphate ($1.67 \pm 0.12 \mu\text{mol/L}$) and silicate ($28.2 \pm 5.3 \mu\text{mol/L}$), with mean values of $\text{SiO}_3^{2-}/\text{PO}_4^{3-}$, N^* and Si^* of 16.8, -11.7 and $16.7 \mu\text{mol/L}$, respectively. The AL contains positive N^* ($0.8 \mu\text{mol/L}$) and negative Si^* ($-5.4 \mu\text{mol/L}$), in contrast to Pacific water. The ADW shows higher concentrations of SiO_3^{2-} and hence $\text{SiO}_3^{2-}/\text{PO}_4^{3-}$, suggesting a contribution by silica recycling. The differences in N^* and Si^* between Canada Basin water layers indicate that nutrient tracers can distinguish Pacific and Atlantic source waters. The vertical distribution of

nutrients indicates that the MH layer can be characterized by N* minimum and Si* maximum. In contrast, Si* minimum and $\text{SiO}_3^{2-}/\text{PO}_4^{3-}$ values below 200 m indicate the distribution of Atlantic warm water.

7.2 Neritic tintinnid community structure and vertical mixing

Tintinnids play an important role in the microbial food web and consist of neritic and oceanic ones biogeographically. Neritic tintinnid species are mainly present in continental shelf areas. Knowing their community structure is thus critical to better understand the ecological function of microzooplankton in the Pacific Arctic Region. During the summer of 2019, neritic tintinnid diversity, vertical distribution, and mixing with oceanic tintinnids were investigated from the Bering Sea to the Chukchi Sea. A total of 19 neritic tintinnid species belonging to 5 genera were identified. All of the neritic species were reported in waters south of the Pacific Arctic Region. No endemic Arctic neritic tintinnid was found. The distributions of nine abundant neritic species exhibited no difference between the Bering Sea and Chukchi Sea. Abundant neritic species were divided into surface- and bottom-dwellers according to their vertical distributions (Figs. 7-2 and 7-3). Bering Shelf Water was dominated by neritic bottom-dwellers, while Anadyr Water was inhabited by neritic surface-dwellers. Neritic and oceanic tintinnids from the Pacific were mainly advected into the Chukchi Sea by Bering Shelf Water. Neritic bottom-dwellers could be mixed into surface waters possibly due to upwelling caused by Pacific Inflow Water flow over shelves. In surface waters, the neritic tintinnid community represented < 50% of the total tintinnid abundance. Our results will help to predict future changes in the microzooplankton community under the influence of global warming and increasing Pacific Inflow Water on the Pacific Arctic Region shelf as well

as in the Arctic basin.

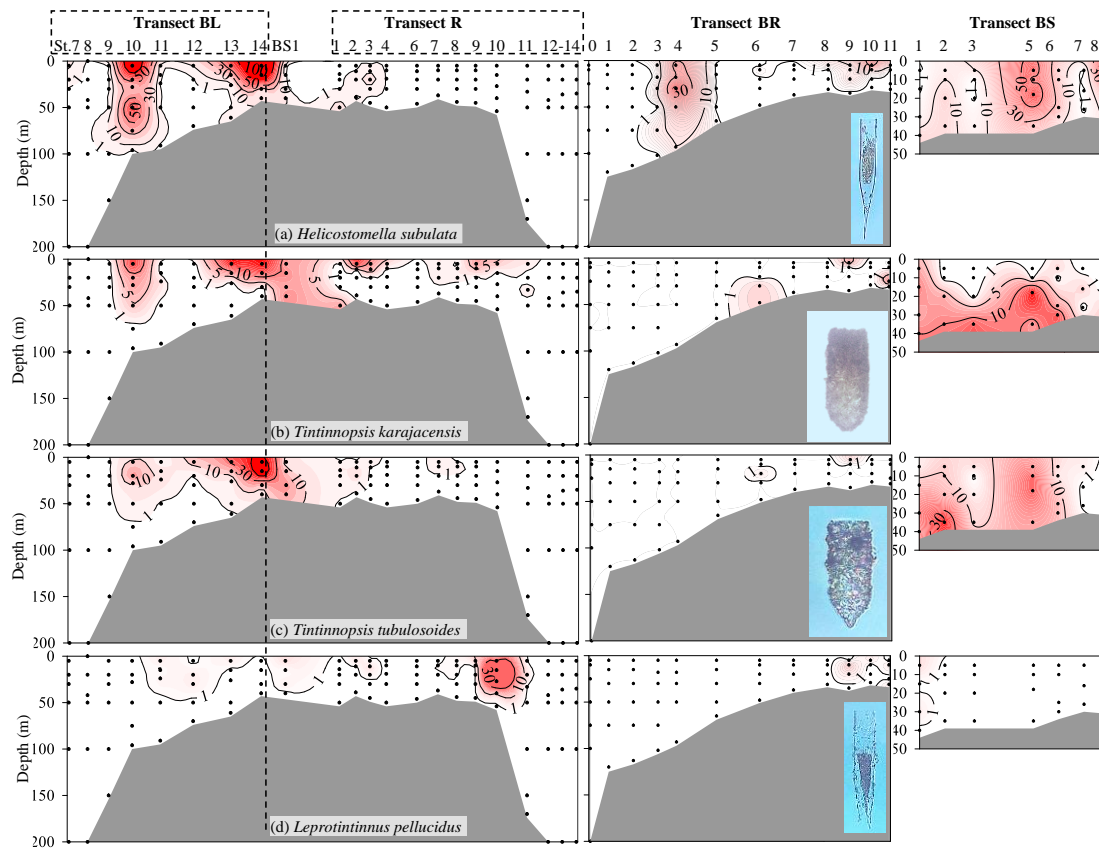


Fig. 7-2. Abundances (ind. L⁻¹) and vertical distributions of surface neritic tintinnid species from the surface to bottom (or 200 m). Black dots: sampling depths; black dotted box: different transects; black dashed line: boundary of the Bering Sea and Bering Strait.

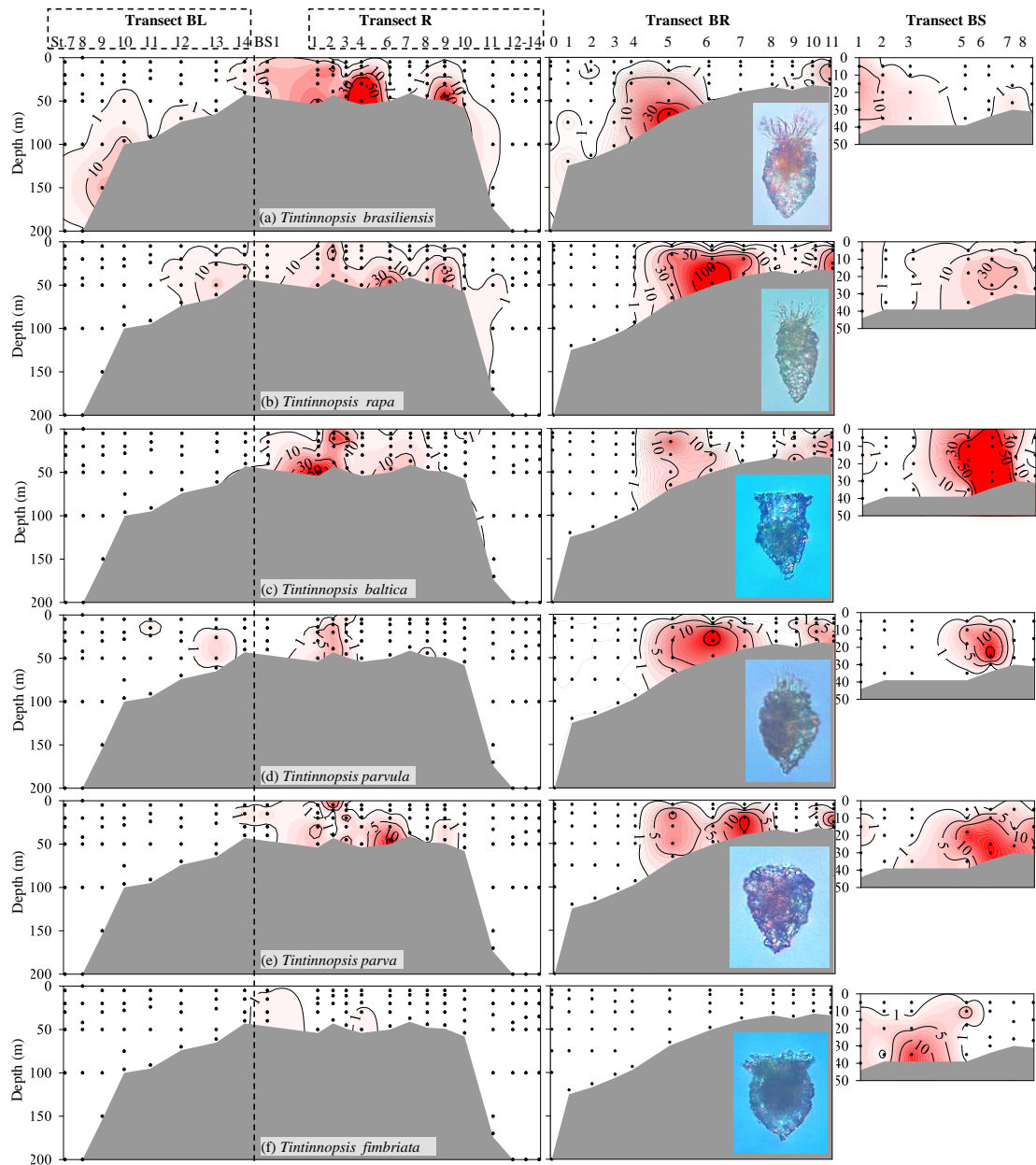


Fig. 7-3. Abundances (ind. L⁻¹) and vertical distributions of bottom neritic tintinnid species from the surface to bottom (or 200 m).

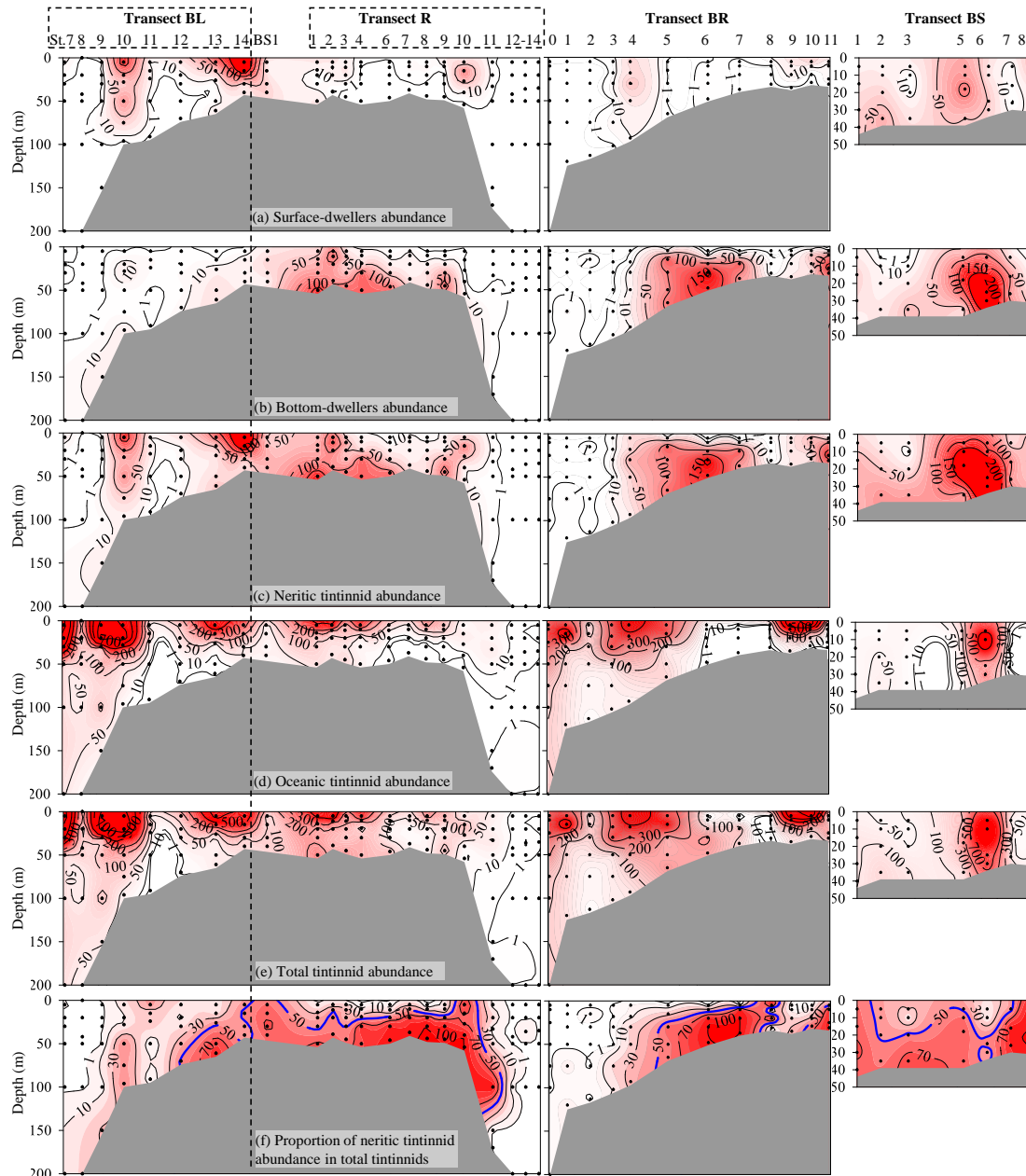


Fig. 7-4. Tintinnid abundances (ind. L⁻¹) (a-e) and proportion (%) of neritic tintinnid abundance in total tintinnids (f) from the surface to bottom (or 200 m).

7.3 Planktonic ciliate community differences in 2016 and 2019

Planktonic ciliates are important component of microzooplankton, but there is limited understanding of their responses to changing environmental conditions in the Pacific Arctic Region. We investigated the variations of ciliate community structure and their relationships with

environmental features in the Pacific Arctic Region in summer 2016 and 2019. The Pacific water was warmer and more saline in 2019 than in 2016. The abundance and biomass of total ciliate and aloricate ciliate were significantly higher in 2019 than those in 2016, while those of tintinnid were significantly lower. The dominant aloricate ciliate changed from large size-fraction (>30 μm) in 2016 to small size-fraction (10-20 μm) in 2019. More tintinnid species belonging to cosmopolitan genera were found in 2019 than in 2016 (Fig. 7-5), and distribution of tintinnid species (*Codonellopsis frigida*, *Ptychocylis obtusa*, and *Salpingella* sp.1) in 2019 expanded 5.9, 5.2 and 8.8 degrees further north of where they occurred in 2016 (Fig. 7-6). The combination of environmental variables revealed that best match with tintinnids were temperature and salinity, while those for aloricate ciliate was temperature. Temperature might play a key role in ciliate distribution. These results provide basic data on the response of planktonic ciliate community to hydrographic variations, and implicated potential response of microzooplankton to Pacification as rapid warming progresses in the Pacific Arctic Region.

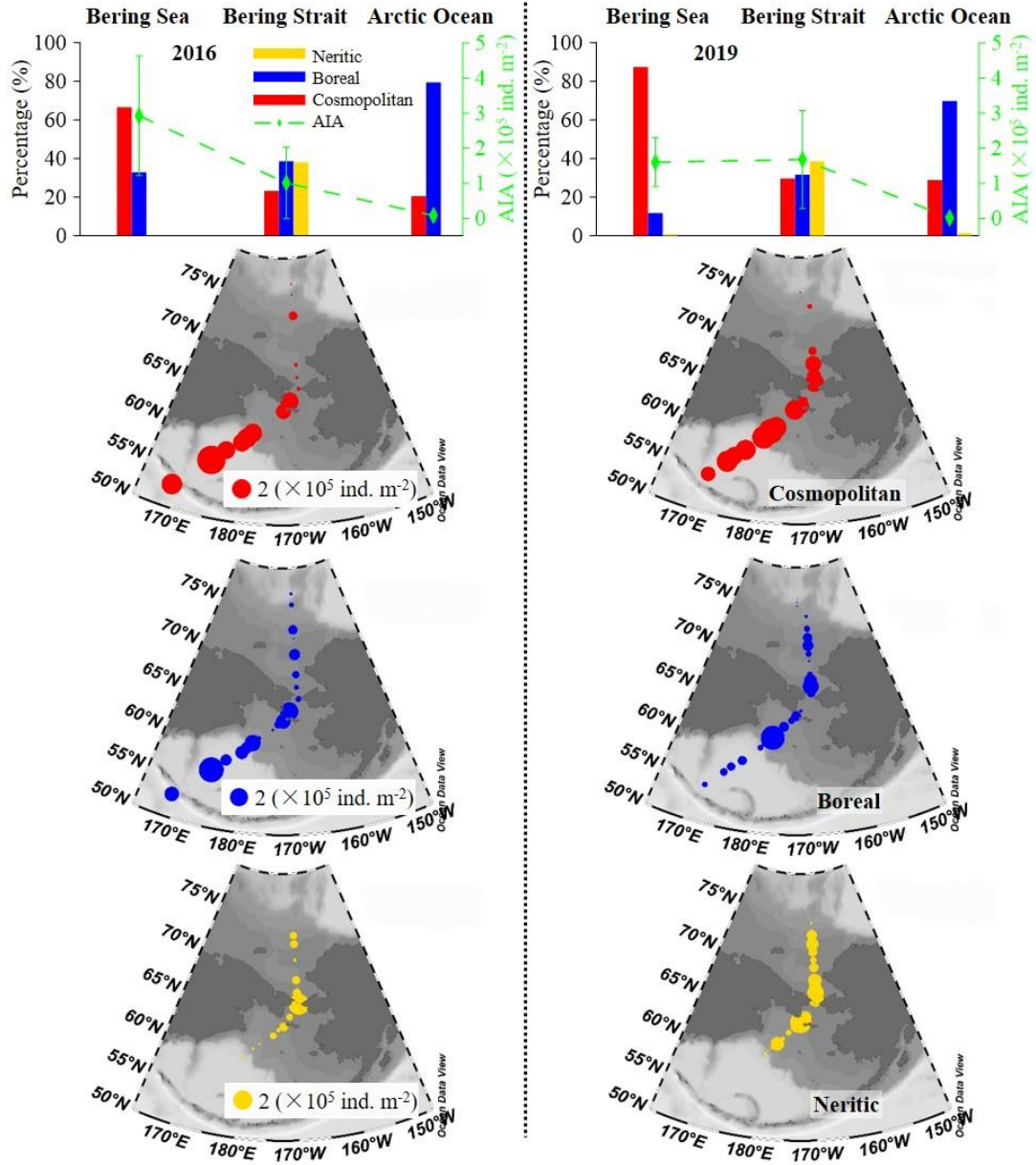


Fig. 7-5. Latitudinal variation of cosmopolitan, neritic and boreal tintinnid (average) integrated abundance and its percentage. AIA, average integrated abundance.

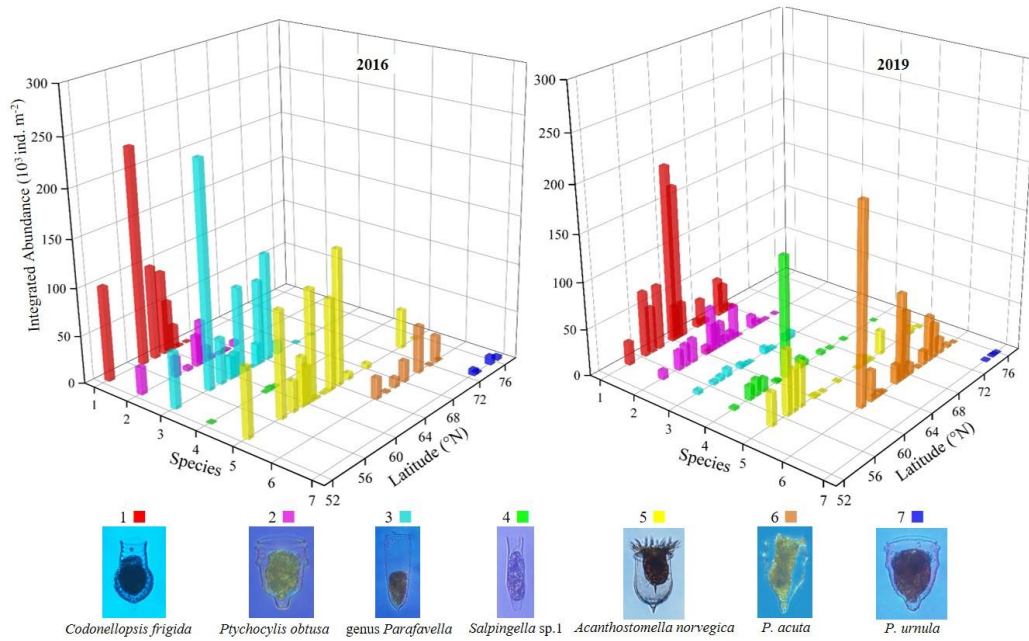


Fig. 7-6. Latitudinal distribution variation of dominant oceanic tintinnid integrated abundance.

7.4 Meridional Variation of picophytoplankton

We analyzed the abundance, cell size and cellular pigments of picophytoplankton from subtropical Pacific to Chukchi Sea by flow cytometry, during the 10th Chinese Arctic expedition. Their responses to environmental factors were also analyzed. *Prochlorococcus* was not detected in any stations and picophytoplankton community was only comprised of *Synechococcus* and pico-eukaryotes, with cell abundance of $(0.1\sim46.7)\times10^3$ cells/mL and $(1.1\sim43.2)\times10^3$ cells/mL, respectively. *Synechococcus* and picoeukaryotes attained higher abundance where nutrient concentrations increased in the continental shelf of Bering Sea. The lowest abundance was observed in Chukchi Sea for *Synechococcus* and in subtropical Pacific for picoeukaryotes (Fig. 7-7). Despite of the

comparable abundance of picoeukaryotes and *Synechococcus*, the former dominated picophytoplankton carbon biomass in the studied area. Both size scattering (related to cell size) and cellular pigments of picophytoplankton varied more than 2 folds, and showed no consistent trends with latitude or temperature (Fig. 7-8). Under similar temperature, nutrient limitation significantly reduced cell size of picophytoplankton. Cell size and cellular pigment were not related with *Synechococcus* but positively related with picoeukaryotes. The results suggested trophic status was another important factor, in addition to temperature, that regulated the cell size of picoeukaryotes and *Synechococcus*.

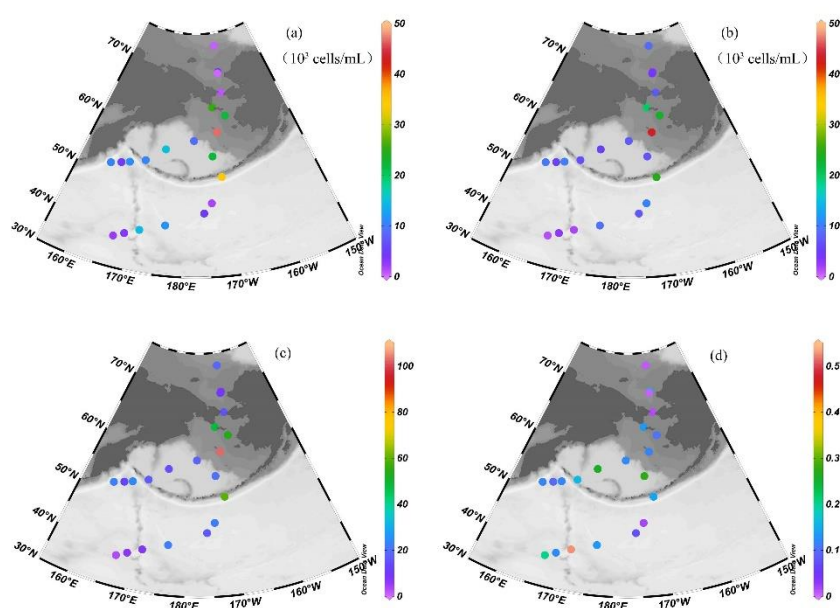


Fig. 7-7 Distribution of (a) *Synechococcus* abundance, (b) picoeukaryotes abundance, (c) total picophytoplankton carbon biomass and (d) proportion of Syn to total picophytoplankton carbon biomass along the marginal seas of northwestern Pacific in summer, 2019

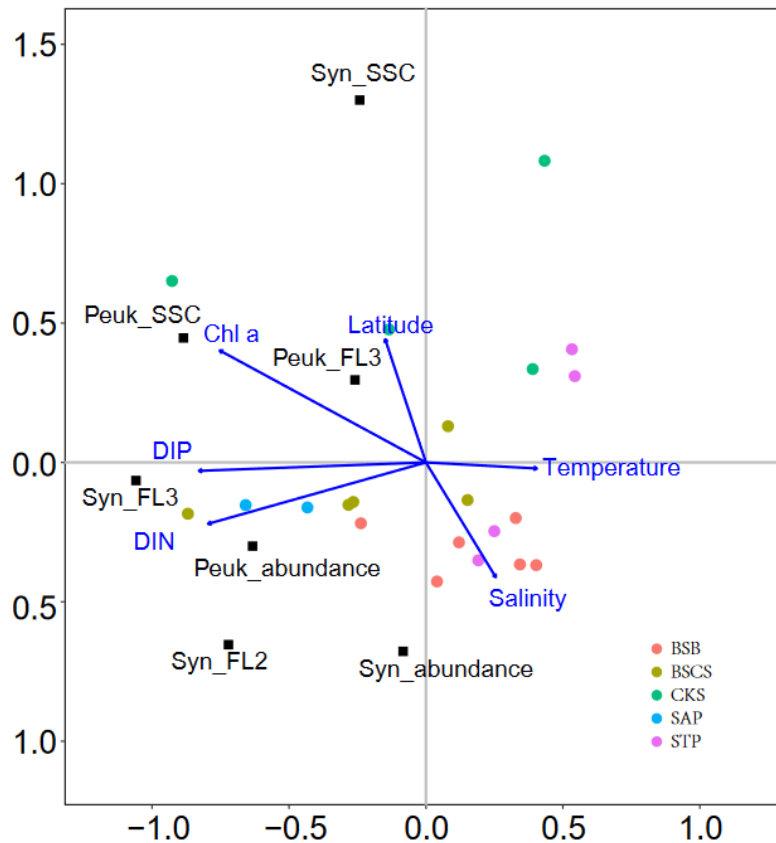


Fig. 7-8 Redundancy analysis between picoplankton abundance and cell optical properties and environmental factors. BSB: Bering Sea Basin; BSCS: Bering Sea Continental Shelf; CKS: Chukchi Sea; SAP: Sub-Arctic Pacific and STP: Sub-tropical Pacific

7.5 Grain size implications for sediment source and sink

The varieties of sediment types and compositions of surface sediments in the study area are caused by sediment erosion, transport, and deposition and reworking in the Bering and Chukchi seas.

As shown in Fig.7-9, three sensitive components: coarse, middle (sortable silt), and fine end-members can be defined by the grain size standard deviation of surface sediments in the Bering and Chukchi seas.

The coarse component (125~2000 μm) from extremely coarse sand to fine sand is difficult to be transported by sea currents in general. Its high contents appear in the area around the Bering Strait (Fig.7-10) and reflect seabed and coastal erosion caused by strong current-the Bering Inflow.

Meanwhile, terrestrial ice floe and sea ice occurred in the cold season is possible to bring coarse sediments into the sea.

The fraction of 16~63 μm represents the sortable silt, which is often transported by currents in the sea. As shown in Fig.7-11, the sortable silt is high on the continental shelves of the Bering and Chukchi seas. It indicated that the sediments on the continental shelves especially in the east of the Bering Sea and the central part of the Chukchi Sea are transported and well-sorted by strong seabed current or circulation.

The fine component <16 μm including fine silt and clay can be transported by weak current and suspension. As shown in Fig.7-12, it is higher in the western side than in the eastern side of the Bering shelf, and higher on the north and south sides of the Herald Shoal in the Chukchi Sea, which indicate a large fraction of mud is derived from the coastal bays and rivers, and then transported and deposited in the area by weak current and suspension.

In words, grain size compositions and sediment types are complex and show differences in sedimentary environment in the Bering Strait, the Bering Sea and the Chukchi Sea (Fig.7-10~ Fig.7-12). They are caused or influenced by bottom relief, hydrodynamic particularities and sediment provenances in these high-latitude areas. Marine circulation in the Bering and Chukchi seas including the Bering Inflow plays important roles in sediment erosion, transport and deposition, but also in hydrological and ecological exchange between the Arctic and the North Pacific oceans, which needs further detail study.

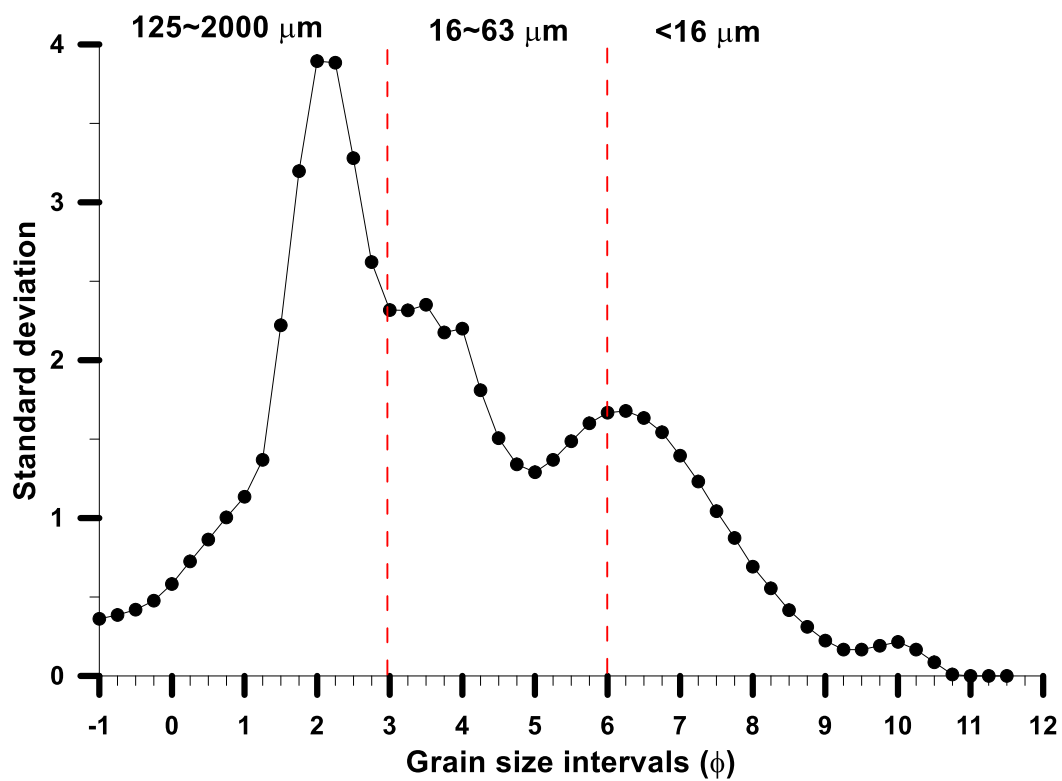


Fig. 7-9 Three components indicated by the grain size standard deviation curve.

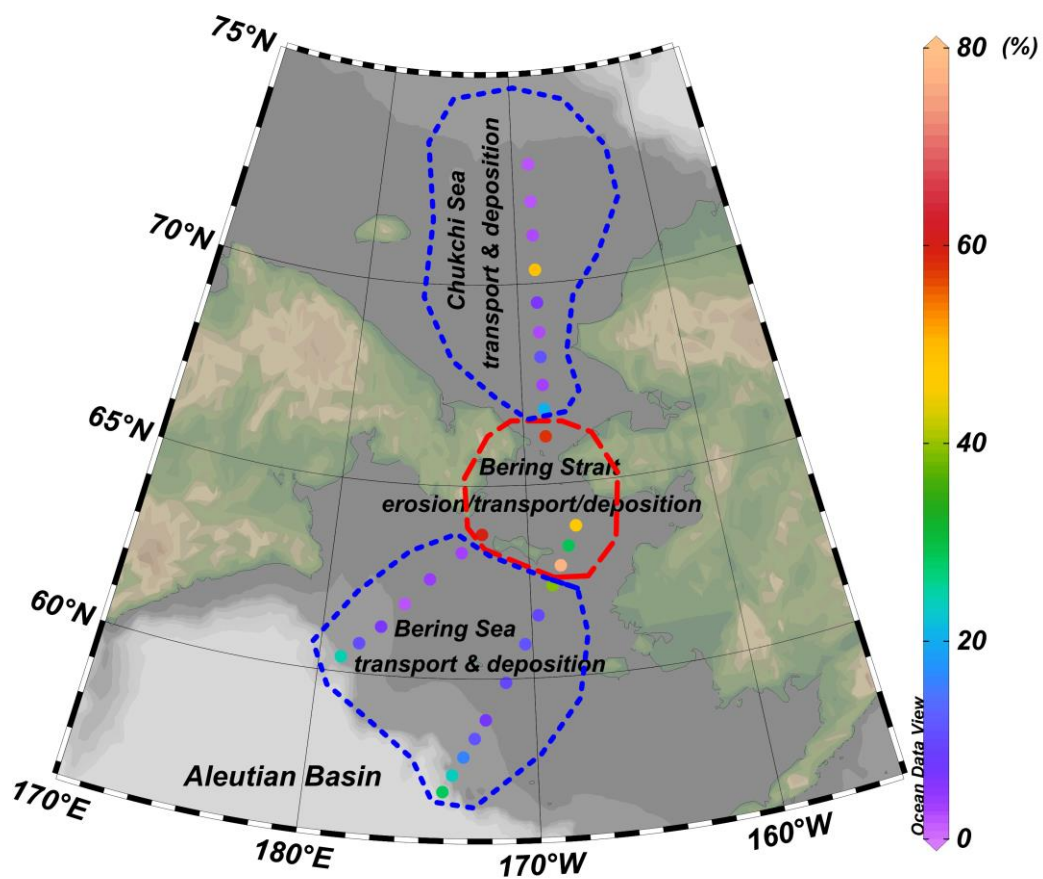


Fig. 7-10 Percentage of the coarse grain size component (125~2000 μm) with

schematic divisions of sedimentary environments in the Bering and Chukchi seas.

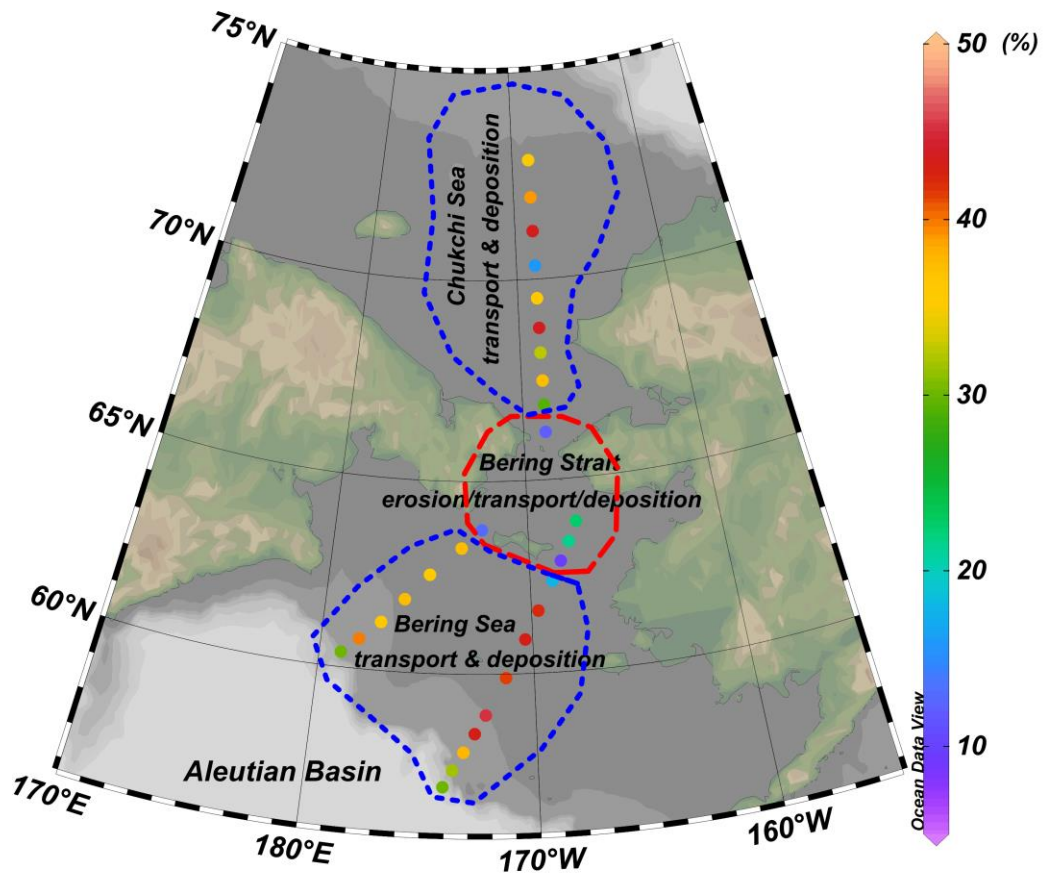


Fig. 7-11 Percentage of the sortable silt (16~63 μm) with schematic divisions of sedimentary environments in the Bering and Chukchi seas.

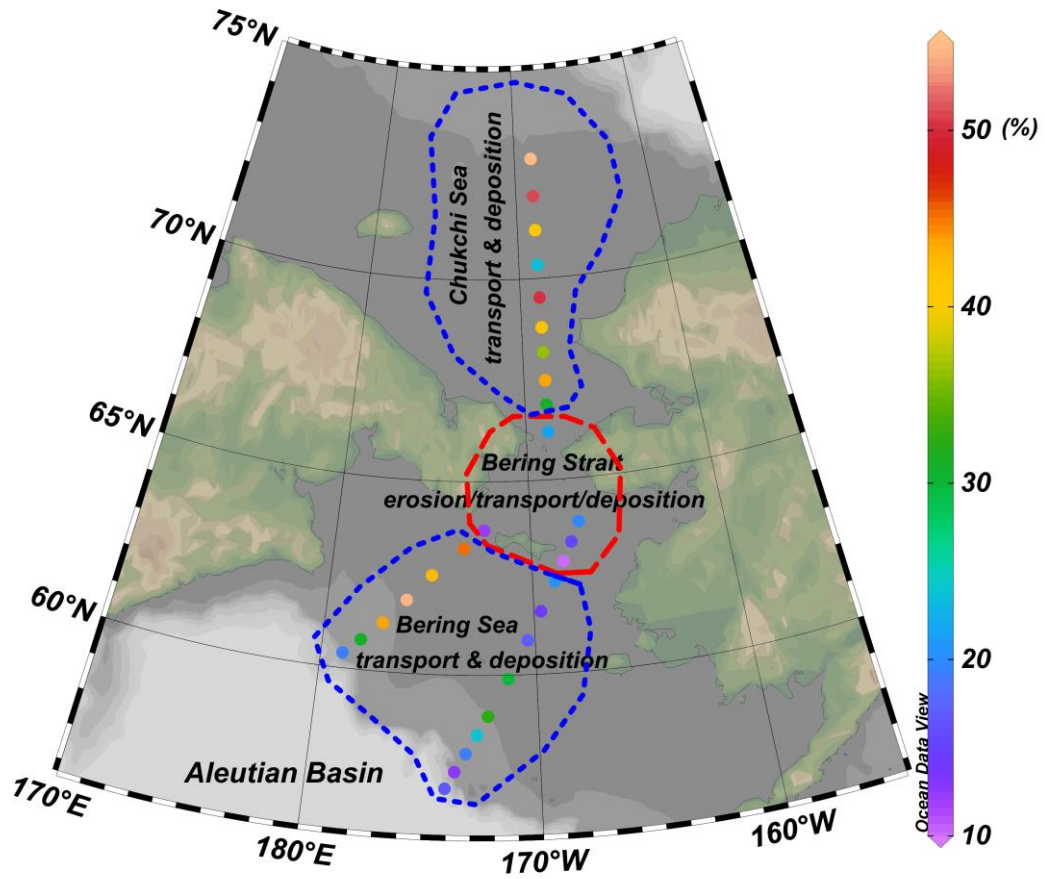


Fig. 7-12 Percentage of the fine grain size component (<16 μm) with schematic divisions of sedimentary environments in the Bering and Chukchi seas.